Reconstructing the Late Cretaceous inversion of the Roer Valley Graben (southern Netherlands) using a new model that integrates burial and provenance history with fission track thermochronology

E. Luijendijk,[1] R. T. Van Balen,[1] M. Ter Voorde,[1] and P. A. M. Andriessen[1]

Received 28 October 2010; revised 11 February 2011; accepted 14 March 2011; published 9 June 2011.

[1] Apatite fission track thermochronology is a powerful tool for the reconstruction of the thermal and geological evolution of sedimentary basins. However, reconstructing basin evolution using thermochronological data is complicated by the fact that sediments also record the thermal history of their source areas. Moreover, samples frequently contain grains from multiple source areas. We have constructed a new numerical model that integrates sediment burial and thermal history with provenance history scenarios and that uses the derived thermal history to calculate synthetic apatite fission track data. We have applied this model to study the evolution of the Roer Valley Graben and to explore the dependency of fission track data on provenance and basin thermal history. Samples that are buried at shallow depths (<1400 m) preserve a mix of late Paleozoic and early Mesozoic provenance ages that correspond to the Caledonian and Variscan orogenic events of the sediment source areas, the London-Brabant and Ardenno-Rhenish massifs, respectively, with varying degrees of subsequent exhumation. Using this knowledge about the inherited thermal history, fission track data of Mesozoic sediments could be used to constrain the Late Cretaceous inversion of the basin with an accuracy of ±250 to ±500 m. These results show that inversion-related exhumation was localized, reaching a maximum of 750 to 1250 m in the eastern part of the basin, while not exceeding 500 m in the western half of the basin. These results are in agreement with the distribution of preserved preinversion sediments and syninversion sediment accumulations that flank the northeastern part of the basin.

Citation: Luijendijk, E., R. T. Van Balen, M. Ter Voorde, and P. A. M. Andriessen (2011), Reconstructing the Late Cretaceous inversion of the Roer Valley Graben (southern Netherlands) using a new model that integrates burial and provenance history with fission track thermochronology, *J. Geophys. Res.*, *116*, B06402, doi:10.1029/2010JB008071.

1. Introduction

[2] The Roer Valley Graben is a Mesozoic-Cenozoic rift system, which following reactivation during the Oligocene forms the northwest extension of the European Cenozoic Rift system [*Geluk*, 1990; *Geluk et al.*, 1994; *Michon et al.*, 2003; *Zijerveld et al.*, 1992], a chain of rift basins in the Alpine and Pyrenean foreland that extends southward to the lower Rhone valley in southern France [*Ziegler*, 1992b; *Dèzes et al.*, 2004]. The Roer Valley Graben has undergone a complex geological and thermal history, owing to basin inversion events during the Late Cretaceous and Paleogene. The timing and the magnitude of a Late Cretaceous phase of inversion in particular has not yet been resolved.

[3] Various explanations for the driving forces of the Late Cretaceous and Paleogene inversion of basins in the European plate and the relation between these phases have been proposed [*Dèzes et al.*, 2004; *Dronkers and Mrozek*, 1991; *Kley and Voigt*, 2008; *Vejbæk and Andersen*, 2002; *Ziegler*, 1987; *Ziegler et al.*, 1995, 1998]. Obtaining accurate estimates of the timing, magnitude and spatial distribution of exhumation is key to untangling the processes responsible for inversion. However, estimates of the amounts of exhumation of the inverted basins in the northwest European plate during the Late Cretaceous and Paleogene vary widely [*Brun and Nalpas*, 1996; *Dronkers and Mrozek*, 1991; *Senglaub et al.*, 2005] and are highly uncertain [*Kockel*, 2003], in part because the relative magnitude of the various inversion phases is difficult to distinguish, due to the erosion of sediments separating them and the lithological similarity between preinversion and postinversion carbonate sediments (see for instance *de Lugt et al.* [2003]).

[4] Previous studies have shown that low-temperature thermochronology is a powerful tool to reconstruct the ther-

[1]Faculty of Earth and Life Sciences, Vrije Universiteit Amsterdam, Amsterdam, Netherlands.

0148-0227/11/2010JB008071

mal and exhumation history of inverted sedimentary basins [*Corcoran and Dore*, 2005; *Gallagher et al.*, 1998; *Green et al.*, 1995; *Japsen et al.*, 2007; *Senglaub et al.*, 2005]. One of the key challenges for interpreting thermochronological data in sedimentary basins is to take into account the inherited thermal signal of the time preceding the deposition of the sample in the basin [*Carter and Gallagher*, 2004; *Rohrman et al.*, 1996; *Van der Beek et al.*, 2006]. The interpretation of thermochronological data in sedimentary basins relies on deriving the temperature history of samples using inverse modeling techniques [*Gallagher et al.*, 1998; *Ketcham*, 2005]. However, applying these techniques to samples that contain a thermal signal from several source areas can lead to unrealistic values for reconstructed temperature histories of the basins studied.

[5] Initial analysis of apatite fission track samples from the Roer Valley Graben [*Green and Duddy*, 1987; *Green*, 1992a, 1992b] yielded nonhomogeneous age distributions that suggest a mixture of fission track age populations. These inhomogeneous age populations could be the result of inherited ages from the two main sediment source areas of the Roer Valley Graben, the London-Brabant Massif and the Ardenno-Rhenish Massif, that were formed during the Caledonian [*Debacker et al.*, 2005] and Variscan [*Littke et al.*, 2000] orogeny, respectively. The dependence of fission track data on both provenance and basin thermal history complicates the interpretation of these data.

[6] We have constructed a new numerical model to derive thermal histories from thermochronological data in basins with mixed sediment source areas. In this model the post-deposition thermal history is combined with a range of preburial thermal histories. These preburial thermal histories represent the range of thermal histories that the various apatite grains have experienced in their source areas, and can be specified or calibrated using inverse modeling techniques. The basin thermal history is calculated using a one-dimensional burial history model. The combined provenance and burial temperature histories are used to simulate the distribution of apatite fission track ages and lengths, which can then be compared to fission track data taken from boreholes. For samples that contain signals from mixed source areas, each simulated temperature path explains a part of the observed variability of fission track age and length distributions.

[7] We have used this model to reconstruct the thermal history of the Roer Valley Graben, focusing in particular on the Late Cretaceous inversion of the basin. The model was calibrated using a data set of 23 apatite fission track samples taken from boreholes in the Roer Valley Graben. Provenance thermal history scenarios were based on known geological history of sediment source areas and observed fission track ages in samples that were buried at shallow depths and did therefore not experience significant burial heating in the basin. In addition, we have calibrated provenance history scenarios of a selected number of samples using inverse modeling techniques, which allowed us to explore the effect of mixed provenance ages on the derived basin thermal history. Estimates of basin inversion that were derived from the model experiments were compared to estimates of the thickness of eroded sections derived from well data and seismics. Finally, we briefly discuss the implications of the provenance thermal history derived from the fission track data for the geological evolution of the sediment source areas, i.e., the London-Brabant and Ardenno-Rhenish massifs.

2. Geological Setting

2.1. Geological Evolution of the Roer Valley Graben

[8] The Roer Valley Graben is located in the southern Netherlands and adjacent parts of Belgium and Germany (Figure 1), and forms the northwestern branch of the European Cenozoic Rift System [*Ziegler*, 1992a]. The Roer Valley Graben formed during the latest Permian and Triassic, as a response to extensional reactivation of deep NW-SE trending faults [*Dirkzwager et al.*, 2000]. Analysis of subsidence records identified two Mesozoic rifting stages, one during the Permian and Early Triassic and one in the Middle Jurassic [*Geluk et al.*, 1994; *Zijerveld et al.*, 1992], which were alternated by periods of thermal subsidence. Inversion of the rift basin during the Late Cretaceous has generated a major angular unconformity that separates Mesozoic sediments from overlying Maastrichtian-Danian deposits. A second unconformity is related to a middle Paleocene phase of basin inversion [*Geluk et al.*, 1994]. Regional subsidence resumed during the late Paleocene and early Eocene. A minor erosional unconformity separates the early Eocene and the Miocene [*Verbeek et al.*, 2002]. The Roer Valley Graben was reactivated as a rift basin during the Oligocene [*Michon et al.*, 2003], with subsidence accelerating during the Pliocene and Pleistocene [*Zijerveld et al.*, 1992].

[9] Up to 3.5 km of Triassic to Lower Cretaceous deposits have accumulated in the rift basin. Triassic deposits are dominated by continental clastic sediments, alternating with evaporites and shallow marine carbonates [*Winstanley*, 1993]. Lower and Middle Jurassic deposits consist of marine sands, shales and carbonates that are classified as the Altena formation. Upper Jurassic and Lower Cretaceous fluvial deposits are part of the Nieuwerkerk formation [*Wong*, 2007; *Herngreen and Wong*, 2007]. Upper Cretaceous carbonate sediments are largely absent in the basin, with the exception of a 10 to 50 m thick formation of Maastrichtian-Danian limestones. Cenozoic deposits are dominated by marine clastic sediments. The reactivation of rifting during the Oligocene and Neogene led to the deposition of up to 1800 m of sediments, consisting of shallow marine deltaic deposits that grade into fluvial deposits during the Pliocene and Pleistocene.

[10] Paleogeographical reconstructions by *Ziegler* [1990] and *Winstanley* [1993] indicate that Mesozoic sediments were mainly derived from the London-Brabant Massif and the Ardenno-Rhenish Massif (Figure 1). From the Triassic to the Middle Jurassic sediments were derived exclusively from these two source areas, while during the Late Jurassic and Early Cretaceous sedimentation was reduced to a narrow chain of rift basins including the Roer Valley Graben. Thus, sediments could additionally have been derived from surrounding highs (Figure 1). During the Late Cretaceous carbonate sediments covered the London-Brabant Massif, which thus ceased to be a sediment source area [*Vandenberghe et al.*, 2004]. During the Cenozoic the Ardenno-Rhenish massif continued to supply sediments [*Ziegler*, 1990]. Alpine detrital components are only observed in the basin following the late Pliocene [*Boenigk*, 2002; *Heumann and Litt*, 2002].

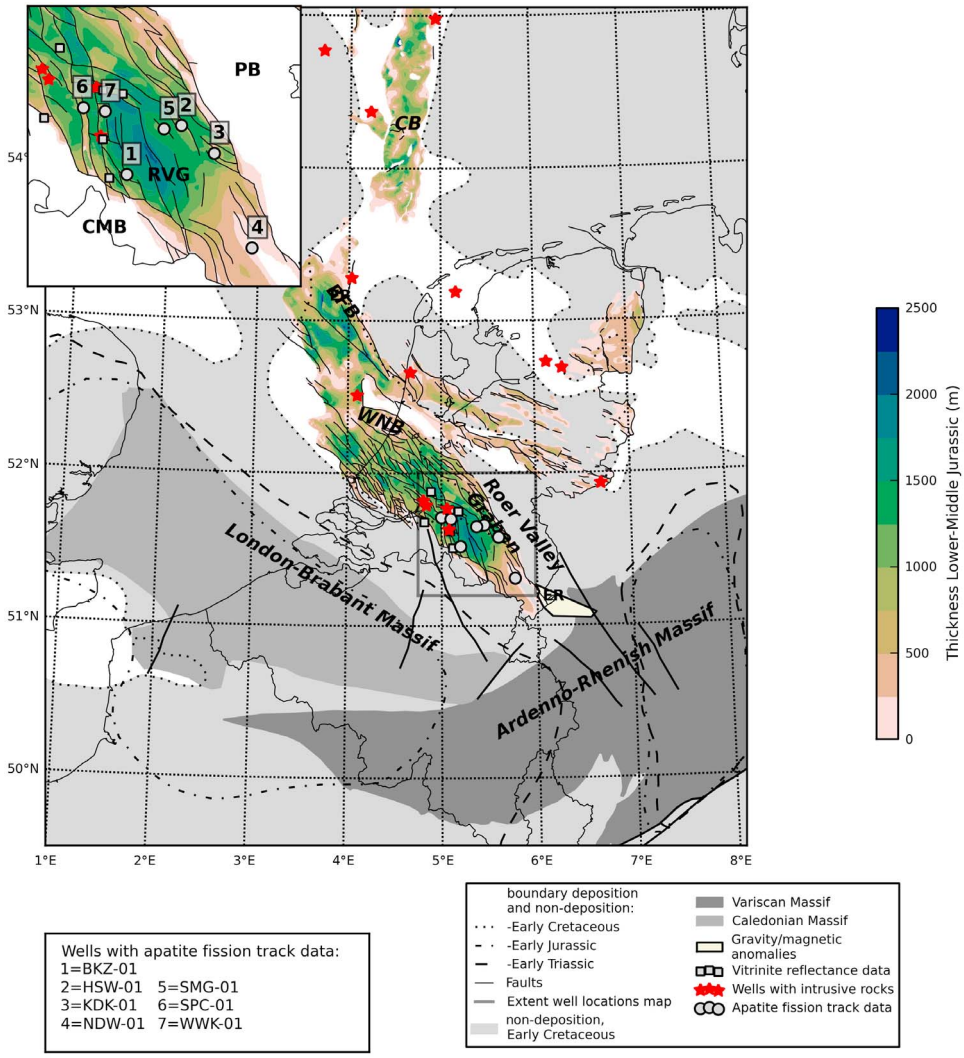

Figure 1. Mesozoic geological setting of the Roer Valley Graben and locations of apatite fission track samples used in this study. The Mesozoic sedimentary basins are shown by the Lower-Middle Jurassic isopach by *Duin et al.* [2006] for the Netherlands onshore and offshore territory. The boundary between deposition and nondeposition during the Early Triassic, Early Jurassic, and Early Cretaceous was based on the work by *Ziegler* [1990]. ER denotes the Erkelenz intrusive [*Bredewout*, 1989]. BFB, Broad Fourteens Basin; CB, central North Sea Basin; CMB, Campine Block; PB, Peel Block; RVG, Roer Valley Graben; WNB, West Netherlands Basin.

2.2. Thermal Evolution

[11] Previous studies of the present-day subsurface temperatures in the Roer Valley Graben have not found a thermal effect of the latest rift phase that started in the Oligocene [*Van Balen et al.*, 2001; *Luijendijk et al.*, 2011]. This is in accordance with the relatively low amount of crustal thinning of approximately 6% to 10% inferred from tectonic subsidence models [*Zijerveld et al.*, 1992], and the modest shallowing of the Moho from 30 km in the structural highs to 27 km in the center of the basin [*Duin et al.*, 1995]. Mesozoic crustal thinning ranges from 5% to 15% during the latest Permian-early Triassic and from 0% to 6% during the Middle Jurassic [*Zijerveld et al.*, 1992]. Model studies suggest that these degrees of thinning would lead to an increase in heat flow of up to 7 mW m^{-2} [*Van Balen et al.*, 2000a]. The low amount of postrift thermal subsidence [*Zijerveld et al.*, 1992; *Van Balen et al.*, 2000a] suggests that rifting was not associated with lithospheric mantle thinning, which would have affected the thermal history of the basin. Similarly, Cenozoic subsidence is entirely caused by fault displacement [*Houtgast and Van Balen*, 2000; *Van Balen et al.*, 2005].

[12] A number of magmatic intrusions near the boundary faults of the rift basin have been inferred from magnetic and gravimetric anomalies and well data (Figure 1). Four wells in the northwest of the Graben and the adjacent West Netherlands basin contain 5 to 50 m thick dikes or sills, which were dated as Lower Cretaceous (125 ± 25 Ma to 133 ± 3 Ma) [*Dixon et al.*, 1981; *Sissingh*, 2004; *Van Bergen and Sissingh*, 2007]. The low-density, 5 km thick and 5 to 10 km deep

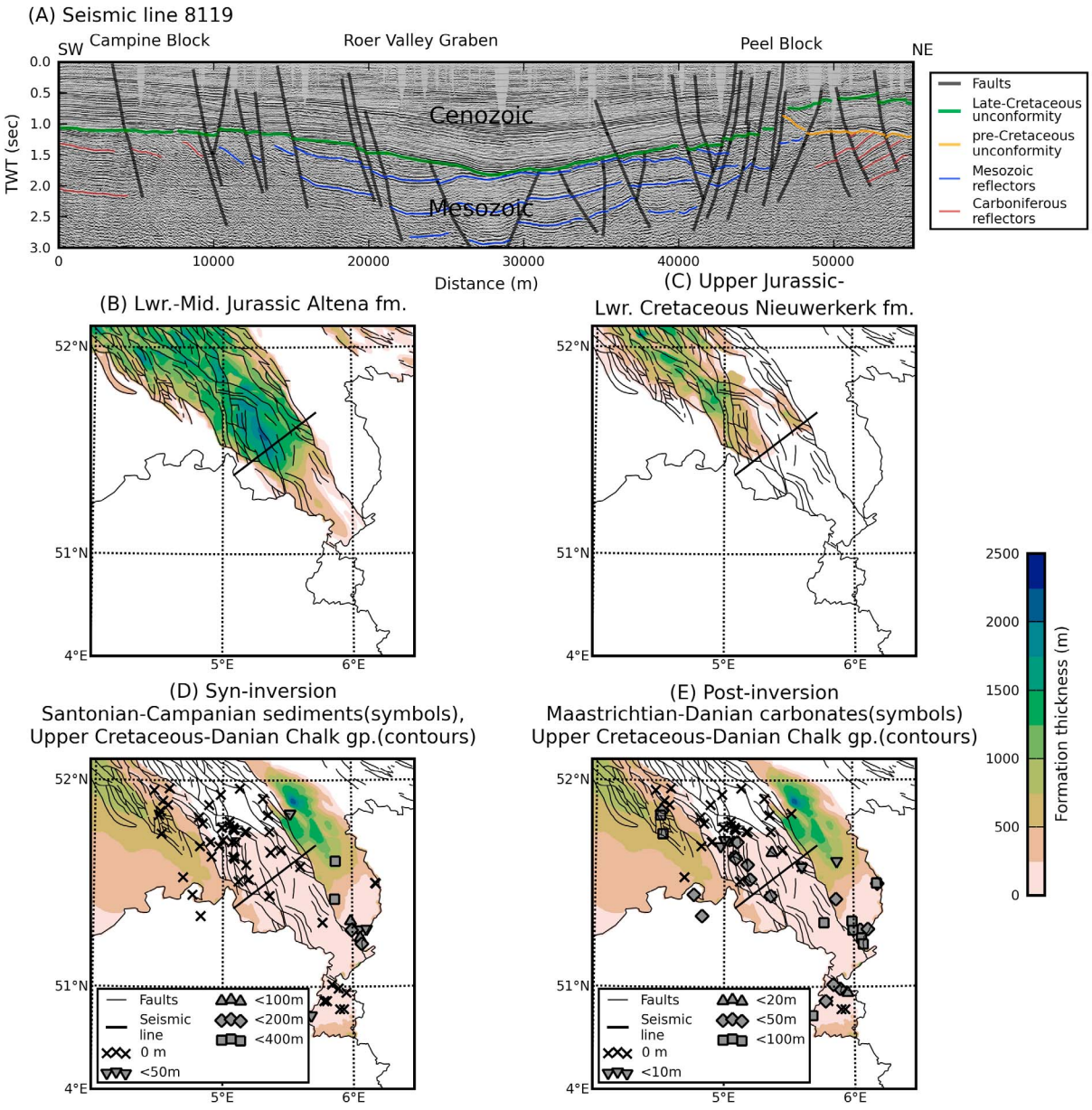

Figure 2. (a) Seismic section perpendicular to the axis of the Roer Valley Graben, showing the angular subcrop of Jurassic and Lower Cretaceous sediments beneath the Late Cretaceous unconformity. (b–e) Thickness distribution of Jurassic, Cretaceous, and early Paleocene sediments deposited before, during, and after the Late Cretaceous (Santonian-Campanian) inversion of the Roer Valley Graben. Based on well data (NL Olie- en Gasportaal, 2010; available at http://www.nlog.nl) and isopach grids by *Duin et al.* [2006], which were based on a dense network of seismic lines [*Van Dalfsen et al.*, 2006].

Erkelenz intrusion has been inferred from a pronounced magnetic and minor gravimetric anomaly [*Bosum*, 1965; *Teichmuller and Teichmuller*, 1971; *Bredewout*, 1989; *Erren and Bredewout*, 1991], with either a Permian [*Van Bergen and Sissingh*, 2007] or a Middle Cretaceous age [*Bredewout*, 1989].

2.3. Basin Inversion

[13] The stratigraphic record of the Roer Valley Graben contains three basin-wide unconformities, dated as Late Cretaceous, middle Paleocene and late Eocene, that have been correlated to the inversion of rift basins in the Northwest European plate [*Gras and Geluk*, 1999; *De Jager*, 2003, 2007; *Japsen et al.*, 2007; *de Lugt et al.*, 2003; *Michon et al.*, 2003; *Nielsen et al.*, 2005; *Van Wijhe*, 1987; *Winstanley*, 1993; *Ziegler*, 1990]. The Late Cretaceous inversion is expressed by folding of the Jurassic and Lower Cretaceous Altena and Nieuwerkerk formations that underly a major unconformity [e.g., *Michon et al.*, 2003; *Winstanley*, 1993], as shown in Figure 2a. The thickness distribution of these

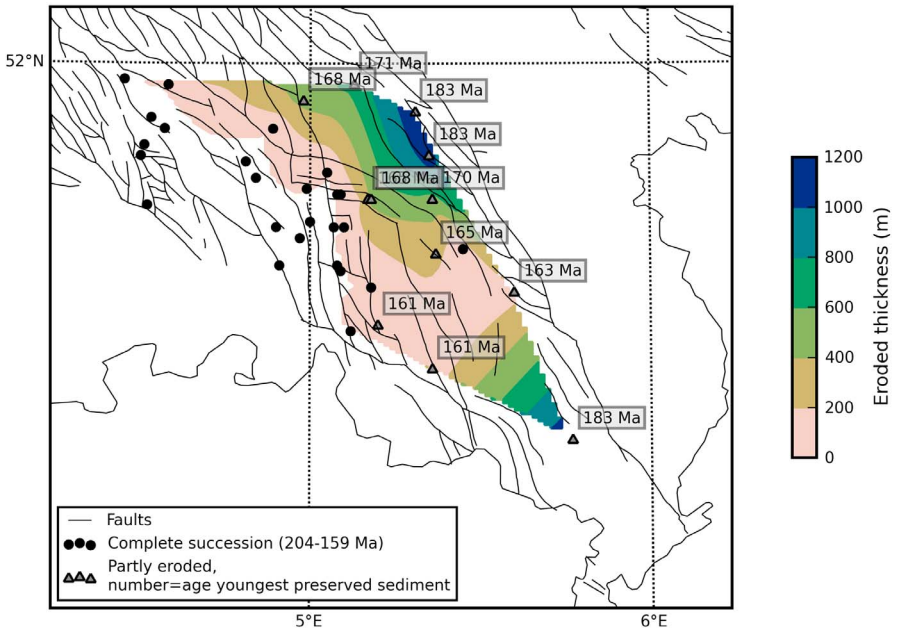

Figure 3. Estimated eroded thickness of the Lower and Middle Jurassic Altena group. These estimates were based on the average thickness of preserved sections in wells located in the Roer Valley Graben. Numbers denote the age of the youngest preserved member of the Altena formation in million years before present.

formations (Figures 2b and 2c) shows pronounced variations, with the thickest deposits of the Nieuwerkerk formation confined to the Northwest of the basin. The truncation of these strata beneath the Late Cretaceous unconformity (Figure 2a) demonstrates that a substantial part of the observed variation in thickness is related to erosion.

[14] Stratigraphic data provide a poor control on the age of the onset of the Late Cretaceous basin inversion. The youngest preserved deposits that underlie the unconformity date from the Berriasian (145.5 to 140.2 Ma [*Van Adrichem Boogaert and Kouwe*, 1997]). In the adjacent structural highs, the onset of basin inversion is marked by the deposition of marine siliciclastic sediments during the Santonian and early Campanian [*Felder*, 1975; *Gras and Geluk*, 1999; *Kuyl*, 1983] (see Figure 2d), for which the uplifted Roer Valley Graben acted as a sediment source [*Bless et al.*, 1993]. The end of the inversion phase is recorded by a transition from siliciclastic to carbonate sediments in the late Maastrichtian [*Felder*, 1996; *Gras and Geluk*, 1999] and the cessation of fault movement on the structural highs [*Kuyl*, 1983], followed by the subsequent relatively uniform deposition of shallow marine carbonates on both the graben and the structural highs (Figure 2e).

[15] A second regional phase of inversion is marked by an unconformity that separates Maastrichtian-Danian limestones of the Houthem formation and a sequence of transgressive sands deposited during the Thanetian [*Van Adrichem Boogaert and Kouwe*, 1997]. The lack of contrast in the thickness of the Houthem formation between the graben and the structural highs (Figure 2e) shows that the magnitude of inversion related erosion during the middle Paleocene was relatively low. However, in the northwestern part of the Graben and the adjacent West Netherlands Basin the Houthem formation is absent (Figure 2e), which could result from substantial erosion during the Middle Paleocene or from nondeposition due to positive topography inherited from the Late Cretaceous basin inversion stage.

[16] The Eocene unconformity is associated with a low value of exhumation (<250 m) [*de Lugt et al.*, 2003; *Michon et al.*, 2003] and is not expressed by an angular subcrop, as shown in Figure 2a.

2.4. Stratigraphic Constraints on Late Cretaceous Exhumation

[17] Paleogeographic reconstructions indicate that the Lower and Middle Jurassic Altena member was deposited with a relatively uniform lithology and thickness in the Netherlands and adjacent regions [*Ziegler*, 1990; *Wong*, 2007]. Therefore, the preserved thickness of this unit was used as a first estimate of erosion during the Late Cretaceous basin inversion phase. The stratigraphic ages of the topmost preserved members of the Altena formation and the estimate of eroded thickness are presented in Figure 3. The thickness of eroded members was calculated as the mean thickness of these units in wells where they have been preserved. The results show that the Altena formation has been preserved in most wells in the Northwest of the graben, indicating that only the overlying Nieuwerkerk formation was eroded during inversion. In contrast, the upper section of the Altena formation is absent in the southern and eastern part of the graben. The strongest erosion was observed in well NDW-01 in the southeastern part of the basin, where only a 20 m thick remnant of this formation is present. This implies an erosion of approximately 1150 m of the Altena formation and an

Table 1. Thermal and Porosity-Depth Parameters Used by the Burial History Model[a]

Lithology	Thermal Conductivity (W m^{-1} K^{-1})	Heat Capacity (J kg^{-1} K^{-1})	Density (Kg m^{-3})	φ_0	c (m^{-1})
Sand	3.5	900	2650	0.3	4.0×10^{-4}
Clay/shale	2.5	900	2720	0.615	9.0×10^{-4}
Carbonate	3.2	900	2710	0.49	7.9×10^{-4}
Evaporite	5.5	900	2500	0.05	0
Pore water	0.65	4300	1025	na	na

[a]Here na means not applicable.

unknown section of Upper Jurassic and Lower Cretaceous deposits prior to the deposition of Maastrichtian-Danian carbonates.

3. Methods

3.1. Burial History Model

[18] The thermal history of the basin was estimated using a one-dimensional burial history model, based on standard backstripping methods [*Bond and Kominz*, 1984; *Steckler and Watts*, 1978]. In this model compaction of sediments is calculated using lithology-dependent exponential porosity-depth coefficients [*Athy*, 1930; *Bond and Kominz*, 1984; *Sclater and Christie*, 1980], using the equation:

$$\phi = \phi_0 e^{-cz} \tag{1}$$

where ϕ is porosity, ϕ_0 is the porosity at the surface, z is depth (m) and c is a porosity-depth parameter (m^{-1}). Values of ϕ_0 and c were calibrated to match porosity data from the study area (Table 1). Burial history was based on detailed well stratigraphy and lithology data provided by the Geological Survey of the Netherlands (NL Olie- en Gasportaal, 2010; available at http://www.nlog.nl). One of the wells (well HSW-01) was drilled through a normal fault. Fault movement was incorporated in the model by adding strata and changing their thicknesses over time, using timing and rate of fault movement based on published well and seismic data [*Duin et al.*, 2006; NL Olie- en Gasportaal, 2010; available at http://www.nlog.nl]. The temperature evolution was calculated using a numerical finite volume solution of the temperature diffusion equation [*Guyer et al.*, 2009], with estimates of the surface temperature and the base heat flux as upper and lower boundary conditions of the model domain. The basal heat flow was calibrated using vitrinite reflectance and fission track data. Surface temperature was based on the work by *Helsen and Langenaeker* [1999]. Thermal diffusivity of the model grid cells was calculated as the geometric mean of the proportions of lithologies and pore water present in the stratigraphic unit [*Clauser and Huenges*, 1995]. The thermal conductivities, heat capacities and densities used to calculate the thermal diffusivity for each lithology are listed in Table 1.

3.2. Inherited Thermal History

[19] The temperature histories derived from the burial history model were combined with end-member scenarios of the provenance thermal history. These end-member scenarios define the range of cooling paths that individual grains experience before being deposited together in a single sample in the Roer Valley Graben. Initial estimates of these provenance history scenarios were based on provenance ages observed in shallow samples that can be assumed not to have been affected by burial heating and exhumation. Further model experiments explored the sensitivity of model results to variation in the assumed provenance ages. For a selected number of samples the ages and cooling rates of these end-member scenarios were calibrated to match the observed fission track data in the study area using the Nelder-Mead Simplex algorithm [*Nelder and Mead*, 1965] as implemented by the SciPy library (E. Jones et al., SciPy: Open source scientific tools for Python, 2010; available at http://www.scipy.org/).

3.3. Model Calibration to Vitrinite Reflectance and Apatite Fission Track Data

[20] The basal heat flow and the magnitude of Late Cretaceous inversion of the Roer Valley Graben were calibrated by matching the modeled and the observed vitrinite reflectance and apatite fission track data. The values of basal heat flow and Late Cretaceous exhumation were calibrated manually using steps of 2 mW m^{-2} and 250 m, respectively.

[21] A total of 201 vitrinite reflectance measurements were available for wells studied [*Integrated Geochemical Interpretation Ltd.*, 1996]. For 44 measurements detailed data were available, which showed that each sample contained on average 11 measurements, with an standard deviation of the R_o value of 0.08. The data of wells SMG-01 and NDW-01 showed unusual scatter, with R_o differences of 0.3 at single depths, and were not used to evaluate model scenarios.

[22] The apatite fission track data set used in this study consists of a set of 23 samples that were obtained from recently released reports for British Petroleum and Clyde Petroleum that have been produced by Geotrack [*Green*, 1992a, 1992b; *Green and Duddy*, 1987]. Table 2 lists the sample details, the location of samples used for apatite fission track analysis is presented in Figure 1. The original reports are available from the website of the Geological Survey of the Netherlands, www.nlog.nl. Fission track ages were determined from the observed density of (spontaneous) fission tracks in apatite grains, and estimates of the ^{238}U concentration of the mineral grain, which were calculated using the external detector [*Gleadow and Lovering*, 1977; *Gleadow*, 1981] and zeta calibration methods [*Hurford and Green*, 1983]. The grains were etched for 20 s in 5M HNO_3 at 20°C. Further information on the analytical procedure can be found in the work by *Green* [1992a, 1992b] and *Green and Duddy* [1987]. For each sample up to 20 apatite grains have used been for the determination of fission track ages and lengths.

[23] Apatite fission track lengths and ages were calculated from the modeled temperature histories using fission track annealing algorithms by *Ketcham et al.* [2000, 2007] and *Ketcham* [2005]. These algorithms are based on a similar etching protocol as the Geotrack data set. Modeled vitrinite reflectance values were calculated using the *Burnham and Sweeney* [1989] EasyRo algorithm.

[24] Previous studies have shown a strong variation in the resistance to annealing of fission tracks between apatite grains, which for a large part can be correlated with the chloride content of these grains [*Barbarand et al.*, 2003;

Table 2. Apatite Fission Track Sample Details[a]

Sample Type	Stratigraphic Age (Ma) Min.	Stratigraphic Age (Ma) Max.	Number of Apatite Grains	N_s	ρ_s (10^6 tracks cm^{-2})	N_i	ρ_i (10^6 tracks cm^{-2})	ρ_D (10^6 tracks cm^{-2})	Zeta	Zeta, Standard Error	Central Age (Ma)	Central Age, Standard Error (Ma)	P (χ^2) (%)	Number of Track Lengths	Mean Track Length (μm)
cuttings	37	28	11	239	2.01	244	2.05	1.55	360	6.8	267.0	25.4	59.0	13	11.2
cuttings	161	159	13	175	0.90	224	1.15	1.59	360	6.8	218.3	23.7	45.0	11	11.5
core	245	244	20	317	0.54	1701	2.90	1.64	360	6.8	40.4	8.4	<1	101	10.1
cuttings	5	1	20	806	2.27	631	1.78	1.73	360	6.8	374.0	39.6	<1	45	12.9
cuttings	23	5	20	365	1.38	259	0.98	1.37	360	6.8	338.2	29.1	51.0	101	11.3
cuttings	164	163	9	272	2.83	121	1.40	1.42	360	6.8	543.4	63.8	23.0	43	12.0
core	245	244	20	1238	1.92	1865	2.89	1.38	360	6.8	167.8	16.6	<1	109	10.4
core	249	249	20	322	1.28	599	2.37	1.38	360	6.8	129.8	13.9	<1	71	10.2
core	249	248	20	105	0.17	1078	1.73	0.82	360	6.8	6.0	3.7	<1	17	9.2
core	251	249	20	59	0.13	952	2.02	1.52	360	6.8	10.0	5.1	<1	0	n/a
core	312	310	20	542	1.14	1345	2.84	1.57	360	6.8	103.4	10.0	<1	107	11.5
core	312	310	20	258	1.18	1085	4.95	1.41	360	6.8	59.8	6.6	<1	104	10.0
cuttings	55	38	14	260	2.33	237	2.13	1.29	360	6.8	225.2	42.0	<1	9	10.8
cuttings	157	134	9	321	0.98	1044	3.52	1.47	354	3.9	151.1	41.3	<1	7	9.1
core	249	248	20	1091	2.78	1328	3.39	1.52	354	3.9	223.2	25.6	<1	106	8.9
cuttings	310	309	20	518	1.54	1039	4.73	1.55	354	3.9	95.2	28.2	<1	40	9.6
cuttings	168	165	20	685	2.10	709	2.17	1.60	354	3.9	267.7	15.6	52.0	40	11.4
core	245	245	20	1375	1.86	3611	4.90	1.63	354	3.9	118.3	18.3	<1	106	10.0
cuttings	248	248	20	369	0.43	3704	4.34	1.65	354	3.9	28.2	6.1	<1	102	9.5
cuttings	163	161	20	506	1.30	428	1.10	1.40	354	3.9	282.7	19.3	75.6	101	13.2
cuttings	165	165	20	635	1.37	640	1.38	1.40	354	3.9	240.4	14.2	4.3	87	12.9
cuttings	245	244	20	76	0.10	1973	2.49	1.40	354	3.9	9.5	1.1	<1	22	7.8
cuttings	249	248	22	432	0.70	2329	3.77	1.40	354	3.9	45.6	2.5	<1	47	8.6

[a]The fission track data were obtained from *Green and Duddy* [1987] and *Green* [1992a, 1992b]. N_s, number of spontaneous tracks; N_i, number of induced tracks; ρ_s, spontaneous track density; ρ_i, induced track density; ρ_D, track density in uranium standard glass. The zeta factor was calculated according to *Hurford and Green* [1983], and the central fission track age was calculated according to *Galbraith and Laslett* [1993].

Carlson et al., 1999; *Green et al.*, 1989; *Ketcham et al.*, 1999, 2007]. Unfortunately, no data on the chloride content or other measures of the annealing resistance of apatites were available for the apatite fission track data set. To account for the unknown chloride content, each model scenario was run using end-member values for the chloride weight content of apatite of 0.1% and 2.0%, respectively. Following *Ketcham et al.* [2007], these end-member scenarios of chloride content can be equated with initial (unannealed) track lengths of 16.21 and 16.55 μm and annealing resistance parameters (r_{mr0} [see *Ketcham et al.*, 2007]) of 0.767 and 0.827. In general, the chloride contents of sedimentary apatites are low, and rarely exceed 2% of the mineral weight [*Carlson et al.*, 1999]. Earlier studies suggest that the chloride content of apatite samples from the Ardenno-Rhenish Massif does not exceed 0.7% [*Glasmacher et al.*, 1998; *Karg et al.*, 2005]. The chloride content does not exceed 1% in a set of 68 samples from Mesozoic sediments in the North Sea basin [*Green*, 1992a].

[25] The fit of the thermal history model to the observed vitrinite and apatite fission track age data was evaluated using z test statistics. The uncertainty of single grain fission track ages was based on the work by *Galbraith* [1984] and *Galbraith and Laslett* [1985]. For the vitrinite reflectance data, the uncertainty of individual measurements was assumed to follow a normal distribution with a standard deviation R_o value of 0.1. As the model was based on end-member scenarios for the provenance thermal history, the test statistic was calculated as the probability that the observed values were equal to any value within the range of simulated end-member fission track age or vitrinite reflectance data. The goodness of fit (GOF) of each fission track sample was calculated as the mean of the probabilities of the single grain measurements. Similarly, the GOF of the vitrinite reflectance was calculated as the mean probability of the individual measurements. Model scenarios were considered acceptable if the GOF of the vitrinite reflectance data and each fission track sample exceeded a value of 0.7. A value of 1 denotes a perfect fit of the model to the observed data. The fit of the track length data was computed as the difference of the mean track lengths of the observed and simulated data. More sophisticated statistical measures such as the Kolmogorov-Smirnov test could not be used, as there was no information available on which apatite grains were used for track length determination for each sample. Given these limitations, model scenarios were primarily evaluated using the fission track age and vitrinite reflectance data.

4. Results

4.1. Inherited Ages

[26] Fission track ages of shallow samples were used to explore the range of ages inherited from sediment source areas. Single grain ages of samples that were buried at depths that did not exceed 1400 m are shown in Figure 4. This burial depth corresponds to a temperature of approximately 60°C, which is generally considered the lower limit of the temperature zone where significant track annealing occurs [*Wagner and Reimer*, 1972]. These samples were derived from Jurassic to Pliocene sediments, yielding 103 single grain ages taken from seven samples.

[27] The geological history of the sediment source areas suggest that most ages would date back to the Caledonian orogeny of the London-Brabant Massif (430–400 Ma) and the Variscan orogeny of the Ardenno-Rhenish Massif (328–305 Ma), as these massifs have remained relatively stable following these orogenic phases [*Ziegler*, 1990]. However, studies of sediment outcrops in the London-Brabant Massif [*Vercoutere and Van den Haute*, 1993] and the Ardenno-Rhenish Massif [*Glasmacher et al.*, 1998; *Karg et al.*, 2005; *Xu et al.*, 2009] have found Mesozoic fission track ages with relatively homogeneous age distributions. The ages of these samples range from 257 to 130 Ma, which is probably related to differential exhumation of these massifs during the Mesozoic [*Glasmacher et al.*, 1998; *Karg et al.*, 2005; *Vercoutere and Van den Haute*, 1993; *Xu et al.*, 2009].

[28] The single grain ages shown in Figure 4 suggest that Caledonian, Variscan and Mesozoic age components are required to explain the inherited ages of the basin's Mesozoic and Cenozoic sediments, although the exact distribution of these components is obscured by the uncertainty ranges of the data. For 99 out of 103 apatite grains fission track ages record a mixed signal of Mesozoic and Paleozoic ages. Six grains have an age range matching the Mesozoic ages found in the source areas, nine grains have an age range spanning the Caledonian and Variscan orogeny, and three grains match only a Caledonian age range. In the remaining grains the uncertainty range covers two or three members of these three age components.

4.2. Model Scenarios of Provenance History

[29] Based on the mixed provenance ages found in Jurassic to Cenozoic samples discussed in section 4.1, and cooling paths in the sediment source areas reported by *Vercoutere and Van den Haute* [1993], *Glasmacher et al.* [1998], *Karg et al.* [2005] and *Xu et al.* [2009] we have defined four end-member provenance history scenarios as an input for further model experiments. These scenarios assume that the apatite grains cooled to temperatures of 120°C during the Caledonian or the Variscan orogeny at 430 to 400 Ma and 328 to 305 Ma, respectively. Each of these two scenarios was combined with two scenarios for the subsequent cooling path: a short, rapid cooling of 10°C Myr^{-1} starting at the beginning of the orogenic phase, after which the grain has remained close to the surface, and a slow, linear cooling lasting from the end of the orogenic phase up to deposition in the Roer Valley Graben. These four end-member scenarios are expected to cover all variability in cooling paths in the sediment source areas arising from variable erosion rates. We refer to this set of provenance thermal histories as the Caledonian-Variscan provenance scenarios. The high uncertainty of single grain ages (Figure 4) and the variation in cooling rates reported by studies in the sediment source areas, do not allow a more detailed subdivision of provenance thermal histories.

4.3. Model Results

4.3.1. Basal Heat Flow and Late Cretaceous Exhumation

[30] An example of the response of simulated apatite fission track and vitrinite reflectance data to burial and provenance history is shown in Figure 5. In these examples we study the amount of exhumation during the Late Cre-

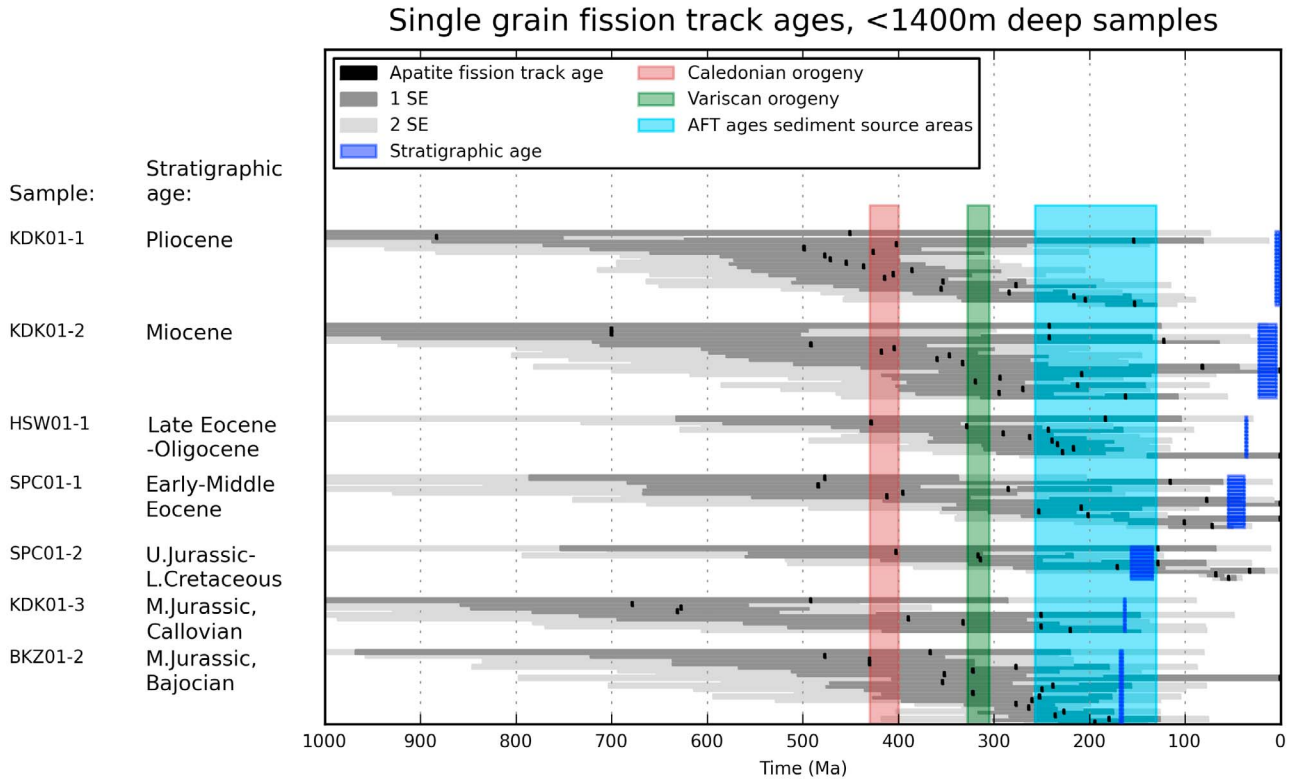

Figure 4. Single grain apatite fission track ages of samples from wells in the Roer Valley Graben that are presently at burial depths of 1400 m or less. Due to their shallow burial in the Roer Valley Graben these samples can be assumed to have remained at temperatures below 60°C and thus have retained their provenance fission track ages. A possible exception is formed by Jurassic and Lower Cretaceous samples that may have been buried deeper than 1400 m before the Late Cretaceous basin inversion. For comparison, the range of apatite fission track ages of outcrop samples in the main sediment source areas of the Roer Valley Graben, the London-Brabant Massif [*Vercoutere and Van den Haute*, 1993] and the Ardenno-Rhenish Massif [*Glasmacher et al.*, 1998; *Karg et al.*, 2005; *Xu et al.*, 2009] is shown in blue. The duration of the main exhumation events of these sediment source areas, the Caledonian and Variscan orogeny, is shown in dark red and green, respectively. SE denotes the standard error.

taceous inversion phase. In Figure 5a, the value of Late Cretaceous exhumation was assumed to be relatively low, 250 m, while for the model scenario shown in Figure 5b an exhumation of 1000 m was assumed.

[31] The model results show an increasingly narrow simulated fission track age range with increasing estimates of basin inversion in the two deepest samples, BKZ01-3 and BKZ01-4. The observed range of single-grain fission track ages in samples BKZ01-3 is 8 to 400 Myr, which indicates that this sample has retained part of its inherited provenance age range. This limits the maximum burial heating attained prior to the Late Cretaceous exhumation phase to values that are lower than shown in Figure 5b. The best model fit was obtained with an exhumation of 250 m (Figure 5a). To match the observed range of fission track ages the full range of provenance history scenarios discussed in section 4.2 was required.

[32] A comparison between modeled and observed temperature, vitrinite reflectance and fission track data for each of the seven wells studied is presented in Figure 6. The model fit of all the values of Late Cretaceous exhumation and basal heat flow that were explored are presented in Figure 7. The statistics of the best fit model scenarios, as well as amounts of exhumation that still result in a good model fit are shown in Table 3. For these model experiments, the basal heat flow was kept at a constant value during the Mesozoic and Cenozoic subsidence history. The thermal history of samples was assumed to be dominated by their burial depths, as the thermal effect of rifting could be assumed to be low (see section 2.2).

[33] For wells BKZ-01, HSW-01, KDK-01, NDW-01 and SMG-01 a good fit of the simulated to the observed vitrinite and fission track data could be obtained using a constant Mesozoic-Cenozoic heat flow (Figure 6). Calibrated values of basin inversion vary from a relatively high value of 1000 m for well KDK-01 to values of 0 to 500 m for the other wells.

[34] Model results of well KDK-01 indicate a relatively high value of Late Cretaceous exhumation, ranging between 750 and 1250 m (Figure 6f). Model experiments that used lower amounts of inversion only provided good model fits in combination with basal heat flows that exceeded 80 mW m^{-2} (Figure 7c). However, bottom hole temperature data suggest heat flow values of approximately 70 mW m^{-2}

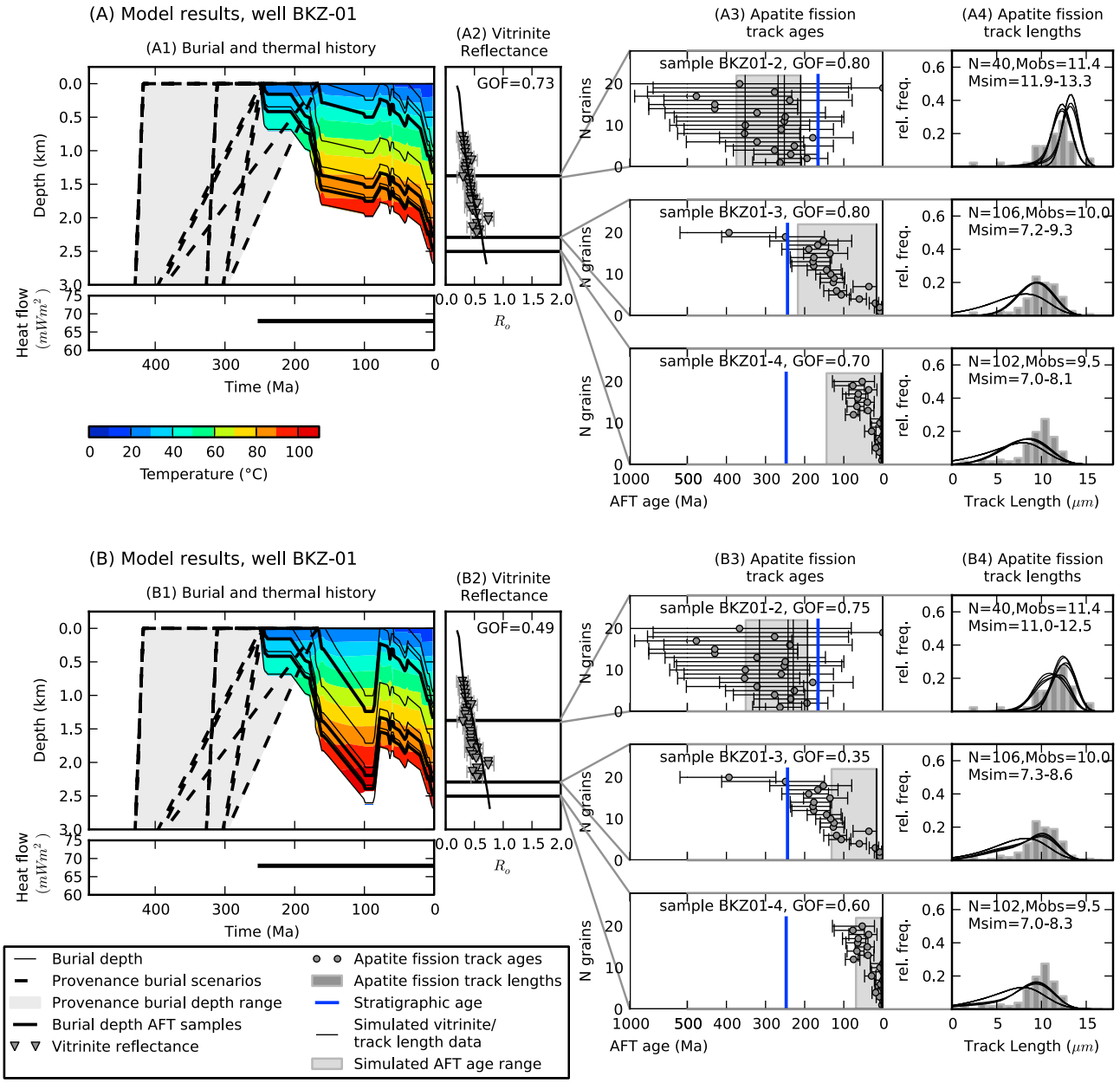

Figure 5. Response of simulated vitrinite reflectance and fission track age and length data of well BKZ-01 to Late Cretaceous exhumation of (a) 250 and (b) 1000 m. The large range of fission track ages observed in sample BKZ01-3 is replicated by Figure 5a, while the deeper burial of Figure 5b reduces ages and narrows the range beyond what was observed in the fission track data. The basal heat flow was kept at a constant value of 68 mW m^{-2} throughout the simulated burial history. The error bars in the fission track age plot denote the ±95% confidence interval. The multiple provenance history and apatite composition scenarios resulted in a number of simulated fission track ages and track lengths distributions. The range of simulated fission track ages is shown by a gray box, while the various simulated track length distributions are shown by gray lines. GOF denotes value of the fit statistic; a value of 1 is a perfect fit of the simulated and the observed data, and a value of 0 means that all of the simulated data fall outside of the uncertainty range of the observed values (see section 3.3). N is the number of measured track lengths. Mobs is the observed mean track length, and Msim is the range of simulated mean track lengths.

(Figure 6f [*Luijendijk et al.*, 2011]). Applying such heat flows required Late Cretaceous exhumation of approximately 1000 m to generate sufficient annealing of fission tracks to match the data. Sample KDK01-3 contains three anomalously high fission track ages (630 Ma to 680 Ma) that did not fit the assumed provenance age scenarios. This sample was not taken into account for further analysis, as including it would have meant that all model scenarios of this well would have to be rejected on the basis of three single grain ages.

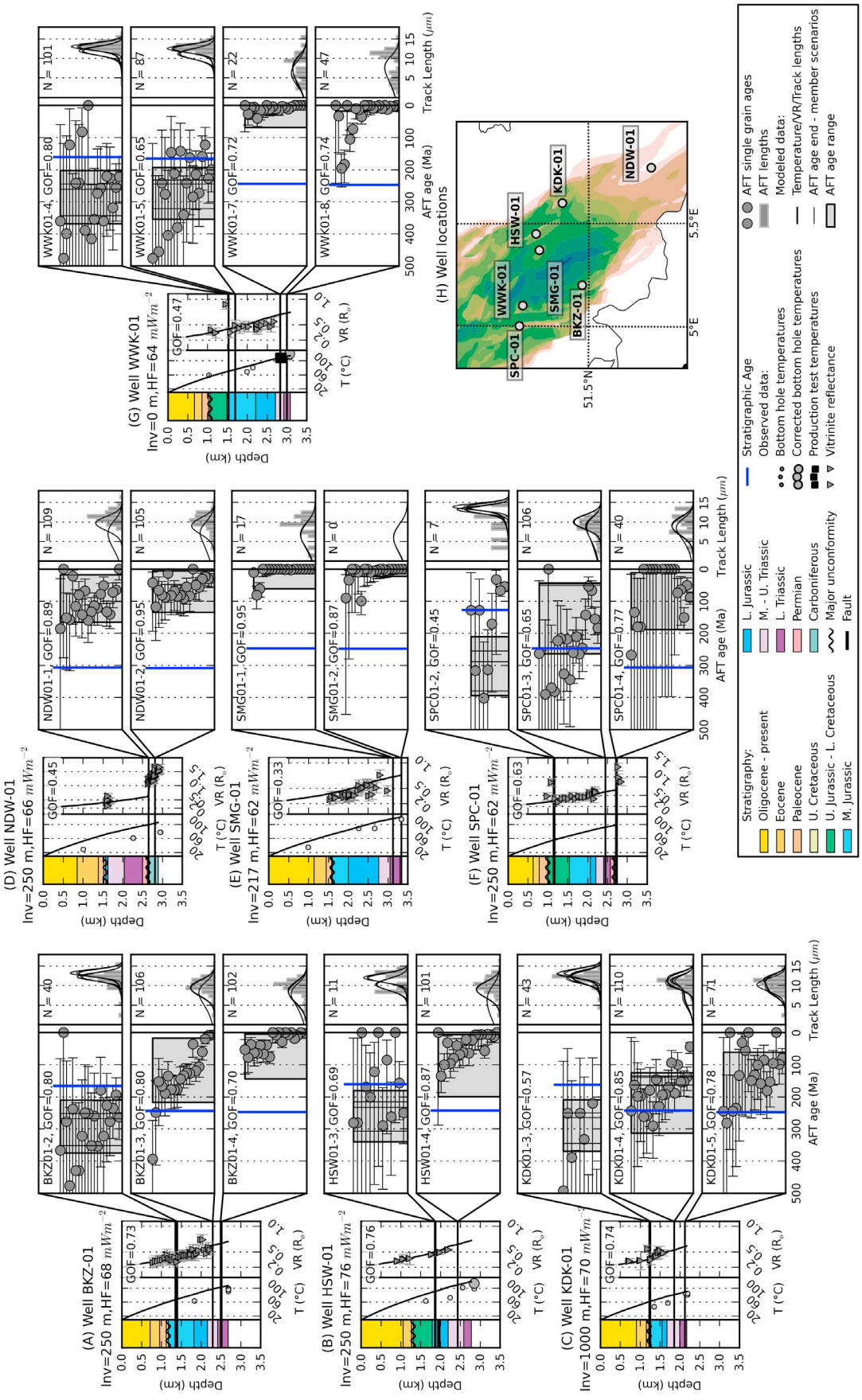

Figure 6. (a–g) Observed and modeled present-day temperature, vitrinite reflectance, and apatite fission track data versus depth for each of the seven wells included in this study. The values of basal heat flow and Late Cretaceous inversion shown are the values that yielded the best fit of all parameter sets that were tried. Apatite fission track samples from Cenozoic stratigraphic units are not shown. GOF, value of the fit statistic; T, present-day temperature; Inv, amount of exhumation during the Late Cretaceous basin inversion phase; HF, basal heat flow; VR, vitrinite reflectance; AFT, apatite fission track.

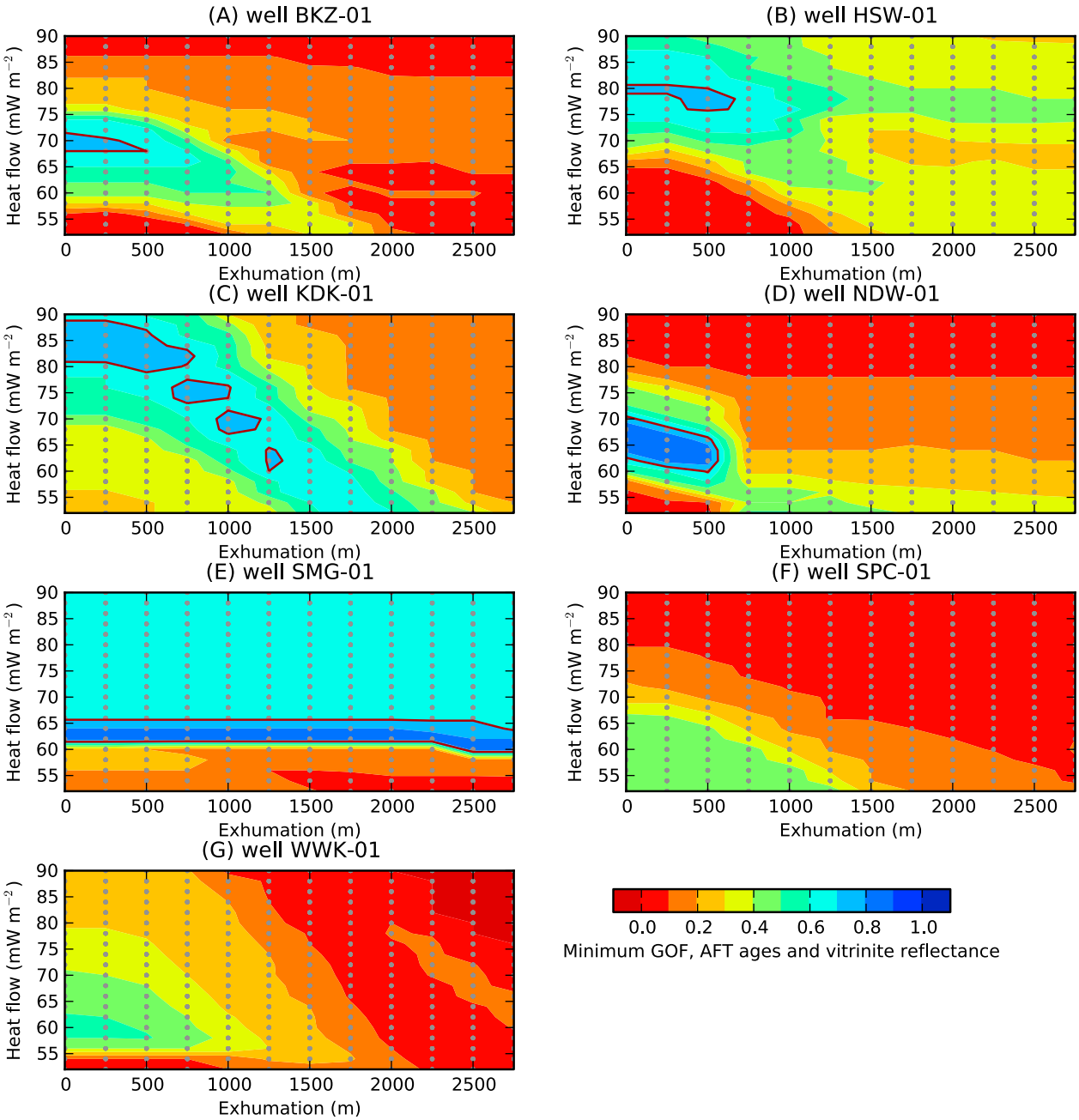

Figure 7. (a-g) Model fit statistics of all Late Cretaceous exhumation and basal heat flow model scenarios. The color contours show the mean goodness of fit for values of the Late Cretaceous exhumation and basal heat flow parameters on the horizontal and vertical axis, respectively. The goodness of fit was calculated by the minimum value of the fit statistic of the vitrinite reflectance and the apatite fission track age data. See section 3.3 for a description of how this fit statistic is calculated. Note that vitrinite reflectance was not used for wells NDW-01 and SMG-01 due to low quality of the data.

[35] Model results of well HSW-01 show that Late Cretaceous exhumation was relatively low at this location, with the best model fit at a value of 250 m (Figure 7b). The calibrated heat flow showed relatively high values of 76 mW m^{-2}. Lower values of heat flow did not yield sufficient reduction of fission track ages to match the low ages of sample HSW01-4, even if higher values of exhumation were applied (Figure 7).

[36] Model experiments of well NDW-01 using exhumation estimates based on the estimated thickness of missing Lower and Middle Jurassic deposits of 1150 m (Figure 3) did not match the fission track data, as the deep burial resulted in resetting of fission track ages that was not observed in the data (Figure 7d). A good fit to the data was only obtained if Late Cretaceous exhumation was limited to values that did not exceed 500 m (Figure 6d). This means

Table 3. Model Calibration Results[a]

Well ID	Estimated Erosion Lower-Middle Jurassic (m)	Thickness Preserved Upper Jurassic–Lower Cretaceous Deposits (m)	Model Scenario	Calibrated Model Parameters		Fit Statistics, Temperature, Vitrinite Reflectance, and Apatite Fission Track Age Data				
				Santonian–Campanian Exhumation (m)	Basal Heat Flow (mW m^{-2})	Temperature	Vitrinite Reflectance	AFT Ages, Average	AFT Ages, Lowest	RMSE Apatite Fission Track Lengths (μm)
BKZ-01	55	0	Best fit	250	68	1.00	0.74	0.77	0.70	0.94
			Min. inversion	0	68	1.00	0.76	0.77	0.70	0.95
			Max. inversion	500	68	1.00	0.71	0.77	0.70	1.05
HSW-01	0	483	Best fit	250	76	0.67	0.76	0.78	0.69	0.84
			Min. inversion	0	80	0.44	0.71	0.82	0.72	1.52
			Max. inversion	500	76	0.65	0.73	0.80	0.71	1.10
KDK-01	110	0	Best fit	1000	70	1.00	0.74	0.73	0.57	0.00
			Min. inversion	750	74	0.73	0.75	0.71	0.57	0.14
			Max. inversion	1250	64	0.78	0.71	0.73	0.57	0.00
NDW-01	1150	0	Best fit	250	66	0.07	0.45	0.85	0.84	0.93
			Min. inversion	0	68	0.04	0.46	0.92	0.89	1.73
			Max. inversion	500	60	0.72	0.44	0.77	0.71	0.93
SMG-01	217	0	Best fit	no constraints	62	1.00	0.36	0.89	0.87	0.00
SPC-01	180	0	Best fit	250	62	na	0.62	0.64	0.45	2.10
WWK-01	0	427	Best fit	0	64	0.72	0.48	0.73	0.65	0.56

[a]For each well, the optimum values of Late Cretaceous exhumation and basal heat flow scenario are shown, as well as the minimum and maximum values of exhumation that resulted in a satisfactory model fit. RMSE denotes the root-mean-square error; na means not available.

that middle Jurassic sediments were probably not deposited in this part of the basin.

[37] Due to their 3.1 to 3.3 km burial, the fission track ages of the two samples of well SMG-01 are mainly determined by the present-day burial heating (Figure 7e), and are independent of their prior burial history. Most of the single grain ages have been reset, while a small number of grains have retained ages of up to 100 Ma (Figure 6b). Such a mix of ages can only be modeled by adopting present-day heat flows of 66 to 72 mW m^{-2}. Higher values would reset all ages, while lower values would not result in any resetting of single grain ages.

[38] The fission track data of wells SPC-01 and WWK-01 did not match fission tracks calculated using the integrated burial and provenance history model. For well SPC-01 this is caused by three out of nine grains in one of the two shallowest samples yielding well-constrained ages that are younger than the Lower Cretaceous stratigraphic age (Figure 6d). The low age is accompanied by a high value of vitrinite reflectance (R_o = 0.84) and relatively short track lengths (mean length is 9.1 μm, N = 7), which indicate that this section has experienced higher temperatures than suggested by the present-day burial depth of 1135 to 1170 m. The relatively high fission track ages of the deeper samples rule out the possibility that these low ages are caused by deeper burial prior to Late Cretaceous basin inversion, and can only be matched by model scenarios where Late Cretaceous exhumation does not exceed 500 m (see Figure 7f).

[39] For well WWK-01, vitrinite reflectance data of this well indicate a relatively low basal heat flow of 52 mW m^{-2}. However, the fission track ages of the Triassic samples WWK01-7 and WWK01-8 require a basal heat flow of at least 64 mW m^{-2} to match the relatively young fission track ages of the two deepest samples (Figure 6a), which is supported by present-day temperature data derived from production tests [*Luijendijk et al.*, 2011]. The cause for this discrepancy is unknown.

4.3.2. Calibrated Provenance Ages

[40] In addition to the model experiments that used fixed end-member provenance scenarios, we have conducted a number of model experiments where the provenance thermal history was calibrated. The results of these experiments are presented in Table 4.

[41] In all cases the calibrated range of ages exceeded the age range of the mixed Caledonian-Variscan provenance scenario that was discussed in section 4.2. This is an additional confirmation that a mixed source area model was necessary to simulate fission track distribution in the Roer Valley Graben. Sample BKZ01-4 forms an exception, as it is mainly controlled by present-day burial temperatures due to its 2.5 km burial depth.

[42] Using calibrated provenance scenarios provided a moderate improvement of the model fit statistic of approximately 10% to 20%. This improvement was sufficient to allow good model fits for model scenarios assuming 1000 m (well BKZ-01) and 1750 m (well KDK-01) of Late Cretaceous exhumation, which exceeds the amount estimated using the Caledonian-Variscan provenance scenarios by 500 m. However, the calibrated provenance ages of these model scenarios ranges from 590 Ma to 950 Ma, which exceeds the Caledonian age (430–400 Ma) expected as an upper provenance age limit from the geological history

Table 4. Calibrated Provenance History End-Member Scenarios of Wells BKZ-01 and KDK-01, Using Various Values for Late Cretaceous Exhumation

	Burial History Model Parameters						Model Fit Statistics				Calibrated End-Member Provenance Scenarios			
							Caledonian-Variscan Provenance Scenario		Calibrated Provenance Scenario		Age of Passing Through 120°C Isotherm (Ma)		Age of Reaching Surface Temperature (Ma)	
Well ID	Santonian-Campanian Exhumation (m)	Basal Heat Flow (mW m^{-2})	Sample ID	Depth (m) Min.	Depth (m) Max.	Stratigraphic Age (Ma)	AFT Ages	AFT Lengths	AFT Ages	AFT Lengths	Min.	Max.	Min.	Max.
BKZ-01	500	68	BKZ01-2	1349	1399	168	0.77	1.05	0.77	0.94	499	476	400	167
			BKZ01-3	2291	2294	245					629	628	292	245
			BKZ01-4	2491	2515	248					248	248	249	248
BKZ-01	1000	64	BKZ01-2	1349	1399	168	0.68	0.76	0.78	0.63	610	448	257	167
			BKZ01-3	2291	2294	245					654	563	287	245
			BKZ01-4	2491	2515	248					249	248	248	248
BKZ-01	1500	54	BKZ01-2	1349	1399	168	0.58	0.06	0.66	0.00	596	595	237	167
			BKZ01-3	2291	2294	245					416	399	409	245
			BKZ01-4	2491	2515	248					249	248	249	248
KDK-01	500	74	KDK01-3	1226	1259	164	0.63	0.31	0.65	0.35	530	426	353	163
			KDK01-4	1859	1859	245					375	375	245	244
			KDK01-5	2126	2126	249					349	326	336	249
KDK-01	1000	70	KDK01-3	1226	1259	164	0.73	0.00	0.75	0.00	452	438	401	163
			KDK01-4	1859	1859	245					396	395	310	244
			KDK01-5	2126	2126	249					426	404	294	249
KDK-01	1750	62	KDK01-3	1226	1259	164	0.51	0.02	0.74	0.44	786	420	737	163
			KDK01-4	1859	1859	245					682	419	424	244
			KDK01-5	2126	2126	249					948	249	600	249

of the London-Brabant Massif. The Caledonian-Variscan provenance age scenarios are supported by the geological history and the fission track data of the sediment source areas and ages of shallow samples in the basin (see section 4.2). Therefore, we have used values of exhumation and basal heat flow derived using these provenance ages for further analysis (Table 3), instead of those using calibrated provenance ages.

5. Discussion

5.1. Model Uncertainties

[43] A large source of uncertainty stems from the number of grains used for the analysis, which is lower than the optimum number of 117 that would be required to capture all populations that exceed a fractional size of 0.05 at a probability of 95% [*Vermeesch*, 2004]. As the sample size of the fission track data set ranges from 9 to 20 grains, there is a relatively high probability that part of the underlying fission track populations have not been captured. Following equation (4) by *Vermeesch* [2004], the theoretical maximum fractional size of the largest unrepresented population ranges from 0.34 for samples with 9 grains to 0.2 for samples containing 20 grains, at a confidence level of 95%.

[44] Rejected model scenarios may have been accepted if more grains would have been counted, and vice versa. The effect is, of course, dependent on the ages of the "missing" population. If we define p_f as the probability that the single grain ages of the unrepresented population are equal to the modeled ages, the two extreme (end-member) possibilities are (1) $p_f = 0$, meaning that the age of the missing population lies entirely out of the range of modeled ages, and (2) $p_f = 1$, meaning that the age of the missing population is equal to the modeled ages. In order to show the possible effect of the missing populations, we adjusted our model fit statistics, assuming both these extreme cases using

$$GOF_{adj} = fp_f + (1 - f)GOF \quad (2)$$

where GOF is the fit statistic calculated for the measured single grain ages, GOF_{adj} is the theoretical fit statistic adjusted for the unrepresented population, f is the fractional size of unrepresented population, p_f is the probability that the single grain ages of the unrepresented population are equal to the modeled ages, which was assumed to be either 0 or 1.

[45] The values of the recalculated fit statistic GOF_{adj} for the model scenarios of two wells, BKZ-01 and KDK-01, are shown in Figure 8. For $p_f = 0$ (Figures 8b and 8d) the fit statistic (GOF_{adj}) of none of the model scenarios exceeds 0.7, which would mean that all scenarios would be rejected. In this case, finding a model with an acceptable fit may require a more complex thermal history, such as histories involving a high temporal variation in basal heat flow or localized thermal anomalies related to igneous activity or hydrothermal flow. However, such histories would be less likely given the geological background information. Conversely, for the case where $p_f = 1$ (Figures 8c and 8e) more model scenarios match the observed fission track data (i.e., $GOF_{adj} >= 0.7$). In this case, the amount of Late Cretaceous exhumation that would be accepted increases by 250 m for both well BKZ-01 and KDK-01.

[46] The results shown in Figure 8 should be considered an approximation of the uncertainty caused by the lower

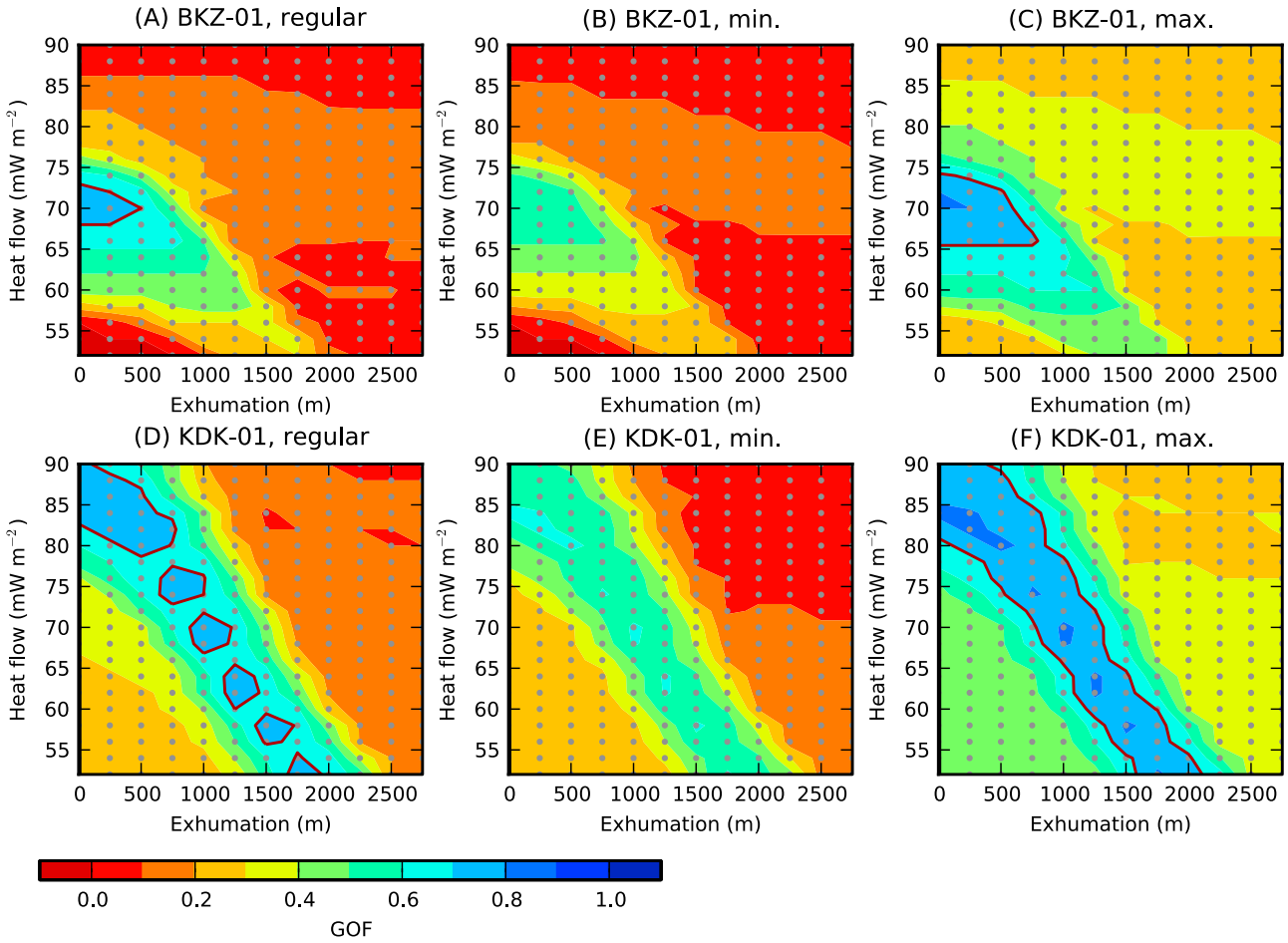

Figure 8. Exploration of the uncertainty of model results caused by the lower than optimal size of fission track samples. Model results for (a) well BKZ-01 and (d) well KDK-01. Model scenarios for well BKZ-01 were constrained by three samples with 20 grains each, while results for well KDK-01 were based on two samples with 20 grains. The model fit statistic (GOF) was computed as the minimum value of the individual GOF of each fission track sample of these wells. In contrast to the results shown in Figure 7 vitrinite reflectance data were not taken into account. (b, c, e, and f) The value of the fit statistic adjusted for a theoretical missing population, i.e., a population that has not been captured by the fission track samples. For Figures 8b and 8e the ages of this population were assumed to fall outside the bounds of modeled fission track ages. Figures 8c and 8f show the model fit assuming that fission track ages of this missing population are equal to the modeled ages.

than optimal grain count. On the one hand, the uncertainty estimate is based on the largest unrepresented population, smaller unrepresented populations may exist that could add uncertainty. On the other hand, the maximum size of the unrepresented population can be considered a worst case scenario; in realistic cases this size is likely to be smaller [*Vermeesch*, 2004]. In addition, the model fit shown in Figure 8 is only based on the fission track ages, without the vitrinite reflectance data that was taken into account in previous model experiments.

5.2. Late Cretaceous Basin Inversion

[47] A comparison of exhumation estimates with the thickness of the preserved Upper Jurassic to Lower Cretaceous deposits and the Upper Cretaceous and Danian Chalk group is shown in Figures 9a and 9b, respectively. The highest value of Late Cretaceous exhumation observed in well KDK-01 coincides with high values of missing of Lower-Middle Jurassic strata shown in Figure 3. However, model results of well NDW-01 suggest that no sediments were deposited in the southern part of the basin during the Middle Jurassic. This shows that the observed distribution of Middle Jurassic deposits in the basin is the result of both nondeposition and Late Cretaceous exhumation. Strong local variations in Late Cretaceous exhumation are suggested by the 750 m difference in exhumation estimates of wells HSW-01 (250 m) and KDK-01 (1000 m), which are located at a distance of 14 km, at approximately equal distance to the boundary faults of the basin. This implies that exhumation was controlled by local differential movement of fault blocks.

[48] The location of the highest value of exhumation in the eastern part of the basin (well KDK-01) is flanked by a 1500 m to 2300 m thick accumulation of the Upper Creta-

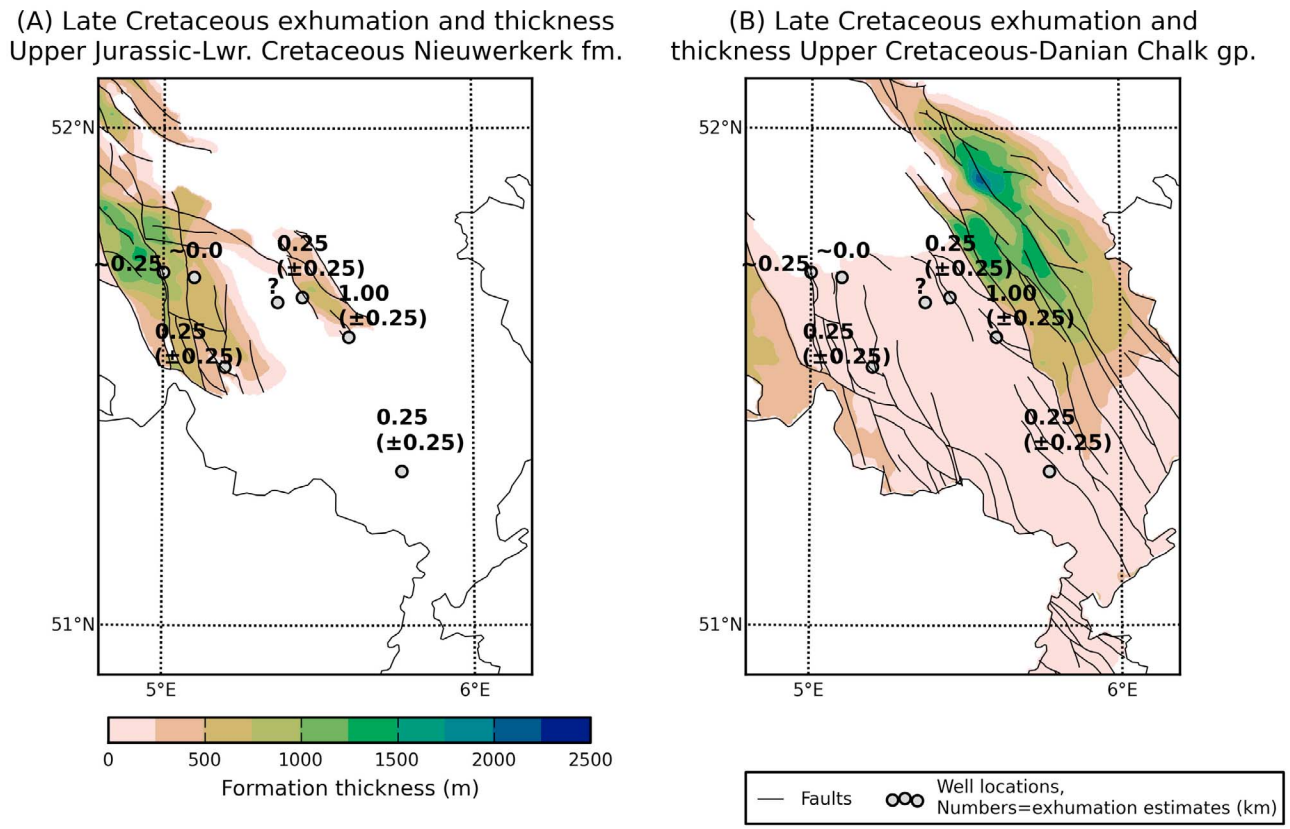

Figure 9. Comparison of the calibrated values of Late Cretaceous exhumation with (a) preserved thickness of the Upper Jurassic and Lower Cretaceous Nieuwerkerk formation and (b) the thickness of the Upper Cretaceous and Danian Chalk group. The estimate of eroded thickness suggest that the Lower Cretaceous fluvial sediments originally extended further south and showed strong local thickness variations that were probably related to fault block motions during deposition. The comparison in Figure 9b suggests a close association of the highest eroded thickness with the highest thickness of preserved Upper Cretaceous deposits along the northeastern boundary fault of the basin.

ceous and Danian Chalk group in a 15 km wide zone northeast of the main boundary fault of the basin (Figure 9b). These deposits are dominated by syninversion Santonian-Campanian clastic sediments [*Gras and Geluk*, 1999]. The structure has previously been interpreted as a marginal trough [*Gras and Geluk*, 1999], which formed by flexural downwarping due to the increased load of the inverted basin [*Nielsen and Hansen*, 2000], like elsewhere in the European plate [*Kockel*, 2003; *Nielsen and Hansen*, 2000; *Nielsen et al.*, 2005]. No corresponding marginal trough has been found in the Campine block to the southwest (Figure 9b), which agrees with the low amount of Late Cretaceous exhumation inferred for wells BKZ-01, SPC-01 and WWK-01 along the western boundary of the basin. The thickness of the supposed marginal trough locally reaches 2300 m, which is more than the maximum estimate of exhumation in the basin (1250 m, well KDK-01; see Table 3). Therefore, it is unlikely that this accumulation can be fully accounted for by flexural downwarping as a response to the load of the inverted Roer Valley Graben. This discrepancy could partly be related to the interaction of intraplate compressive stress with flexural downwarping, which tends to amplify vertical movement of faulted crust [*Van Balen et al.*, 1998]. Additional explanations could be folding or trusting of strata within the Chalk group, which would be difficult to observe using seismic data due to the lack of strong internal reflectors [*Van Adrichem Boogaert and Kouwe*, 1997].

5.3. Implications for the Geological Evolution of Sediment Source Areas

[49] The sediments of the Roer Valley Graben contain a mix of Mesozoic, Variscan and Caledonian inherited provenance ages (Figure 4). The prevalence of this mixed age signal throughout the Mesozoic-Cenozoic sedimentary fill shows that the configuration of sediment source areas and the basin has remained relatively stable. This agrees with paleogeographical reconstructions that indicate that the sediments were sourced from the London-Brabant and Ardenno-Rhenish massifs, which were formed during the Caledonian and Variscan orogeny [*Debacker et al.*, 2005; *Littke et al.*, 2000] and have subsequently been stable highs during the Mesozoic and most of the Cenozoic [*Ziegler*, 1990].

[50] However, fission track studies of outcrops in the sediment source areas have predominantly yielded relatively homogeneous post-Variscan ages [*Glasmacher et al.*, 1998; *Karg et al.*, 2005; *Vercoutere and Van den Haute*, 1993; *Xu*

et al., 2009]. These Mesozoic ages have been linked to exhumation events that eroded a Carboniferous sedimentary cover [*Vercoutere and Van den Haute*, 1993; *Glasmacher et al.*, 1998] and to Jurassic hydrothermal activity [*Glasmacher et al.*, 1998; *Muchez*, 1995]. The discrepancy between the Paleozoic ages found in the basin and the Mesozoic fission track ages in the sediment source areas could indicate that sediments in the Roer Valley Graben have partly been derived from intermediate basins, such as the Campine Basin (see Figure 1 for location). These sediments would not have been affected by the Mesozoic exhumation or thermal events of the massifs and thus have preserved their Caledonian or Variscan fission track age. Alternatively, the Mesozoic fission track ages of the Rhenish Massif could have been the result of the strong Pleistocene exhumation of this massif [*Demoulin et al.*, 2009; *Garcia-Castellanos et al.*, 2000; *Meyer and Stets*, 1998; *Van Balen et al.*, 2000b], which would mean that samples currently at the surface have been subjected to deeper burial and have experienced fission track annealing up to the Pleistocene. Such an event would not show up in the fission track samples studied in the Roer Valley Graben, as the youngest sample that was included in this study dates back to the Pliocene.

6. Conclusions

[51] The influence of provenance thermal history on the ability to reconstruct basin thermal histories from apatite fission track thermochronology was explored using a new model that integrates basin and provenance thermal history. This model was used to reconstruct exhumation during Late Cretaceous inversion of the Roer Valley Graben.

[52] Provenance ages of apatite grains in the Roer Valley Graben were assessed by analysis of Lower Cretaceous and Cenozoic samples that are presently at temperatures lower than 60°C, and have therefore undergone no or limited track annealing after deposition. The observed variation in provenance ages can be explained as a result of ages that have been reset during the Caledonian (430 to 400 Ma) and Variscan (328 to 305 Ma) orogeny of the main sediment source areas, the London-Brabant and Ardenno-Rhenish massifs, with additional age reduction due to the subsequent slow exhumation of these source areas during the Mesozoic.

[53] Model experiments show that the range of fission track ages observed in samples can be an indicator of the burial history experienced by a sample. Samples that have not experienced deep burial have retained their inherited provenance age range, while samples that have been fully thermally reset during burial show a narrow, homogeneous range of ages. The degree of narrowing and reduction of fission track ages could therefore be used as a tool to infer the basin's thermal history. This allows conclusions to be drawn from the interpretation of samples with heterogeneous age populations, that have previously often been considered as complicating factors in the extraction of thermal histories from thermochronological data in basins.

[54] Relatively accurate estimates of Late Cretaceous exhumation could be obtained where a number of samples from different depths was available. The deepest samples constrained the temperatures reached during the most recent, Oligocene to present, burial phase. Shallower Mesozoic samples provide a record of the maximum burial heating prior to Late Cretaceous basin inversion. Combining these data with vitrinite reflectance records allowed the Late Cretaceous exhumation to be determined with an accuracy of ±250 to ±500 m.

[55] In five out of seven wells both the vitrinite reflectance and the fission track data could be simulated using a constant Mesozoic-Cenozoic basal heat flow of 58 to 76 mW m^{-2}. This suggest a limited thermal effect of rifting, which is in accordance with the low rate of Mesozoic-Cenozoic crustal stretching [*Zijerveld et al.*, 1992] and the inferred passive mode of rifting during the Cenozoic [*Luijendijk et al.*, 2011; *Van Balen et al.*, 2001]. Partially reset ages and high vitrinite reflectance values in a single sample in well SPC-01 near the western boundary of the basin could suggest local heat flow anomalies. Sample WWK-01 shows a discrepancy between deep fission track samples that require a high heat flow and relatively low vitrinite reflectance values in overlying strata. However, the data do not allow strong conclusions, as the inferred local thermal effect is based on a low number of samples and apatite grains.

[56] Model simulations of Late Cretaceous basin inversion that were calibrated using vitrine reflectance and apatite fission track data suggest a strong variation in exhumation in the Roer Valley Graben, with the strongest exhumation of up to 1000 ± 250 m confined to a well in the eastern part of the rift basin. Wells in the western and northwestern part of the basin show values ranging between 0 and 500 m. These results, combined with erosion estimates from stratigraphic constraints suggest that the main deformation was confined to the northeastern boundary fault of the Graben, the Peel Boundary Fault. In addition, the inferred pattern of deformation corresponds well to the position of up to 2 km thick accumulation of syninversion deposits at the northeastern flank of the rift basin, which has previously been interpreted as a marginal trough.

[57] **Acknowledgments.** This study was funded by the Dutch Council for Scientific Research (NWO-ALW) grant 815.01.13. This is the Netherlands Research School of Sedimentary Geology publication 20110201. The authors would like to thank Wintershall Noordzee B.V., Northern Petroleum, and Geotrack International for access to the apatite fission track data. We would like to thank Michiel Dusar and two anonymous reviewers for their detailed and helpful comments.

References

Athy, L. F. (1930), Density, porosity, and compaction of sedimentary rocks, *Am. Assoc. Pet. Geol. Bull.*, *14*(1), 1–24.

Barbarand, J., T. Hurford, and A. Carter (2003), Variation in apatite fission-track length measurement: Implications for thermal history modelling, *Chem. Geol.*, *198*(1–2), 77–106, doi:10.1016/S0009-2541(02)00423-0.

Bless, M. J. M., M. Dusar, P. J. Felder, and R. Swennen (1993), Lithology and biostratigraphy of Upper Cretaceous–Paleocene carbonates in the Molenbeersel borehole (NE Belgium), *Geol. Mijnbouw*, *71*, 239–257.

Boenigk, W. (2002), The Pleistocene drainage pattern in the Lower Rhine Basin, *Neth. J. Geosci.*, *81*(2), 201–209.

Bond, G. C., and M. A. Kominz (1984), Construction of tectonic subsidence curves for the early Paleozoic miogeocline, southern Canadian Rocky Mountains: Implications for subsidence mechanisms, age of breakup, and crustal thinning, *Geol. Soc. Am. Bull.*, *95*(2), 155–173.

Bosum, W. (1965), Interpretation magnetischer Anomalien durch dreidimensionale Modellkörper zur Klärung geologischer Probleme, *Geol. Jahrb.*, *83*, 667–680.

Bredewout, J. W. (1989), The character of the Erkelenz intrusive as derived from geophysical data, *Geol. Mijnbouw*, *68*, 445–454.

Brun, J. P., and T. Nalpas (1996), Graben inversion in nature and experiments, *Tectonics*, *15*(3), 677–687.

Burnham, A. K., and J. J. Sweeney (1989), A chemical kinetic model of vitrinite maturation and reflectance, *Geochim. Cosmochim. Acta*, *53*(10), 2649–2657.

Carlson, W. D., R. A. Donelick, and R. A. Ketcham (1999), Variability of apatite fission-track annealing kinetics: I. Experimental results, *Am. Mineral.*, *84*, 1213–1223.

Carter, A., and K. Gallagher (2004), Characterizing the significance of provenance on the inference of thermal history models from apatite fission-track data—A synthetic data study, in *Detrital Thermochronology: Provenance Analysis, Exhumation, and Landscape Evolution of Mountain Belts*, edited by M. Bernet and C. Spiegel, pp. 7–23, Geol. Soc. of Am., Boulder, Colo.

Clauser, C., and E. Huenges (1995), Thermal conductivity of rocks and minerals, in *Rock Physics and Phase Relations: A Handbook of Physical Constants*, *AGU Ref. Shelf*, vol. 3, edited by T. J. Ahrens, pp. 105–126, AGU, Washington, D. C.

Corcoran, D., and A. Dore (2005), A review of techniques for the estimation of magnitude and timing of exhumation in offshore basins, *Earth Sci. Rev.*, *72*(3–4), 129–168, doi:10.1016/j.earscirev.2005.05.003.

Debacker, T. N., S. Dewaele, M. Sintubin, J. Verniers, P. Muchez, and A. Boven (2005), Timing and duration of the progressive deformation of the Brabant Massif, Belgium, *Geol. Belg.*, *8*(4), 20–34.

De Jager, J. (2003), Inverted basins in the Netherlands, similarities and differences, *Neth. J. Geosci.*, *82*(4), 355–366.

De Jager, J. (2007), Geological development, in *Geology of the Netherlands*, edited by T. E. Wong, D. A. Batjes, and J. De Jager, pp. 5–26, R. Neth. Acad. of Arts and Sci., Amsterdam.

de Lugt, I. R., J. Van Wees, and T. E. Wong (2003), The tectonic evolution of the southern Dutch North Sea during the Palaeogene: Basin inversion in distinct pulses, *Tectonophysics*, *373*(1–4), 141–159, doi:10.1016/S0040-1951(03)00284-1.

Demoulin, A., E. Hallot, and G. Rixhon (2009), Amount and controls of the Quaternary denudation in the Ardennes massif (western Europe), *Earth Surf. Processes Landforms*, *34*(11), 1487–1496, doi:10.1002/esp.1834.

Dèzes, P., S. M. Schmid, and P. A. Ziegler (2004), Evolution of the European Cenozoic Rift System: Interaction of the Alpine and Pyrenean orogens with their foreland lithosphere, *Tectonophysics*, *389*(1–2), 1–33, doi:10.1016/j.tecto.2004.06.011.

Dirkzwager, J. B., J. Van Wees, S. A. P. L. Cloetingh, M. C. Geluk, B. Dost, and F. Beekman (2000), Geo-mechanical and rheological modelling of upper crustal faults and their near-surface expression in the Netherlands, *Global Planet. Change*, *27*(1–4), 67–88, doi:10.1016/S0921-8181(01)00060-1.

Dixon, J. E., J. G. Fitton, and R. T. Frost (1981), The tectonic significance of post-Carboniferous igneous activity in the North Sea Basin, in *Petroleum Geology of the Continental Shelf of North-West Europe: Proceedings of the Second Conference on Petroleum Geology of the Continental Shelf of North-West Europe*, edited by L. V. Illing and G. D. Hobson, pp. 121–137, Heyden, London.

Dronkers, A., and F. Mrozek (1991), Inverted basins of the Netherlands, *First Break*, *9*(9), 409–425.

Duin, E., R. Rijkers, and G. Remmelts (1995), Deep seismic reflections in the Netherlands, an overview, *Geol. Mijnbouw*, *74*, 191–197.

Duin, E. J. T., J. C. Doornenbal, R. H. B. Rijkers, J. W. Verbeek, and T. E. Wong (2006), Subsurface structure of the Netherlands—Results of recent onshore and offshore mapping, *Neth. J. Geosci.*, *85*(4), 245–276.

Erren, H., and J. W. Bredewout (1991), Model calculations on intrusive cooling and related coalification of the Peel-Erkelenz coalfield (the Netherlands and Germany), *Geol. Mijnbouw*, *70*, 243–252.

Felder, P. (1996), The Vijlen chalk member (Maastrichtian, Late Cretaceous) in the Meuse-Rhine Euroregion, *Ann. Soc. Geol. Belg.*, *T 119*, 119–133.

Felder, W. (1975), Lithostratigrafie van het Boven-Krijt en het Dano-Montien in Zuid-Limburg en het aangrenzende gebied, in *Toelichting bij de Geologische Overzichtskaarten van Nederland*, edited by W. Zagwijn and C. Van Staalduinen, pp. 63–72, Rijks Geol. Dienst, Haarlem, Netherlands.

Galbraith, R. F. (1984), On statistical estimation in fission track dating, *Math. Geol.*, *16*(7), 653–669.

Galbraith, R. F., and G. M. Laslett (1985), Some remarks on statistical estimation in fission-track dating, *Nucl. Tracks*, *10*, 361–363.

Galbraith, R. F., and G. M. Laslett (1993), Statistical models for mixed fission track ages, *Nucl. Tracks Radiat. Meas.*, *21*(4), 459–470, doi:10.1016/1359-0189(93)90185-C.

Gallagher, K., R. Brown, and C. Johnson (1998), Fission track analysis and its applications to geological problems, *Annu. Rev. Earth Planet. Sci.*, *26*(1), 519–572.

Garcia-Castellanos, D., S. A. P. L. Cloetingh, and R. T. Van Balen (2000), Modelling the Middle Pleistocene uplift in the Ardennes-Rhenish Massif: Thermo-mechanical weakening under the Eifel?, *Global Planet. Change*, *27*(1–4), 39–52, doi:10.1016/S0921-8181(01)00058-3.

Geluk, M. C. (1990), The Cenozoic Roer Valley Graben, southern Netherlands, *Meded. Rijks Geol. Dienst*, *44*, 65–72.

Geluk, M. C., E. J. T. Duin, M. Dusar, R. H. B. Rijkers, M. W. Van Den Berg, and P. Van Rooijen (1994), Stratigraphy and tectonics of the Roer Valley Graben, *Geol. Mijnbouw*, *73*, 129–141.

Glasmacher, U., M. Zentilli, and A. Grist (1998), Apatite fission track thermochronology of Paleozoic sandstones and the hill-intrusion, northern Linksrheinisches Schiefergebirge, Germany, in *Advances in Fission-Track Geochronology*, *Solid Earth Sci. Libr.*, vol. 10, edited by P. van den Haute and F. de Corte, pp. 151–172, Kluwer Acad., Dordrecht, Netherlands.

Gleadow, A. (1981), Fission-track dating methods: What are the real alternatives?, *Nucl. Tracks*, *5*, 3–14, doi:10.1016/0191-278X(81)90021-4.

Gleadow, A., and J. F. Lovering (1977), Geometry factor for external detectors in fission track dating, *Nucl. Track Detect.*, *1*(2), 99–106, doi:10.1016/0145-224X(77)90003-5.

Gras, R., and M. C. Geluk (1999), Late Cretaceous–Early Tertiary sedimentation and tectonic inversion in the southern Netherlands, *Geol. Mijnbouw*, *78*, 1–19.

Green, P. F. (1992a), Thermal history reconstruction in four onshore Netherlands wells using apatite fission track analysis and vitrinite reflectance, technical report, Geotrack Int., Melbourne, Vic., Australia.

Green, P. F. (1992b), Thermal history reconstruction in two onshore Netherlands wells using apaptite fission track analysis and vitrinite reflectance, technical report, Geotrack Int., Melbourne, Vic., Australia.

Green, P. F., and I. R. Duddy (1987), Apatite fission track analysis of samples from Waalwijk-1, Netherlands, technical report, Geotrack Int., Melbourne, Vic., Australia.

Green, P. F., I. R. Duddy, G. M. Laslett, K. A. Hegarty, A. Gleadow, and J. F. Lovering (1989), Thermal annealing of fission tracks in apatite 4. Quantitative modelling techniques and extension to geological timescales, *Chem. Geol.*, *79*(2), 155–182, doi:10.1016/0168-9622(89)90018-3.

Green, P. F., I. R. Duddy, and R. J. Bray (1995), Applications of thermal history reconstruction in inverted basins, *Geol. Soc. Spec. Publ.*, *88*(1), 149–165.

Guyer, J. E., D. Wheeler, and J. A. Warren (2009), FiPy: Partial differential equations with Python, *Comput. Sci. Eng.*, *11*(3), 6–15.

Helsen, S., and V. Langenaeker (1999), *Burial History and Coalification Modelling of Westphalian Strata in the Eastern Campine Basin (Northern Belgium)*, *Geol. Surv. Belgium Prof. Pap.*, vol. 289, 23 pp., Mainjot, Brussels.

Herngreen, G. F. W., and T. E. Wong (2007), Cretaceous, in *Geology of the Netherlands*, edited by T. E. Wong, D. A. J. Batjes, and J. De Jager, pp. 127–150, R. Neth. Acad. of Arts and Sci., Amsterdam.

Heumann, G., and T. Litt (2002), Stratigraphy and paleoecology of the Late Pliocene and Early Pleistocene in the open-cast mine Hambach (Lower Rhine Basin), *Neth. J. Geosci.*, *81*(2), 193–199.

Houtgast, R. F., and R. T. Van Balen (2000), Neotectonics of the Roer Valley Rift System, the Netherlands, *Global Planet. Change*, *27*(1–4), 131–146.

Hurford, A. J., and P. F. Green (1983), Zeta age calibration of fission-track dating, *Chem. Geol.*, *1*(4), 285–317.

Integrated Geochemical Interpretation Ltd. (1996), Geochemical elements of the petroleum system in the greater Waalwijk field area, south Netherlands, technical report, Bideford, U. K.

Japsen, P., P. F. Green, L. H. Nielsen, E. S. Rasmussen, and T. Bidstrup (2007), Mesozoic-Cenozoic exhumation events in the eastern North Sea Basin: A multi-disciplinary study based on palaeothermal, palaeoburial, stratigraphic and seismic data, *Basin Res.*, *19*(4), 451–490, doi:10.1111/j.1365-2117.2007.00329.x.

Karg, H., A. Carter, M. R. Brix, and R. Littke (2005), Late- and post-Variscan cooling and exhumation history of the northern Rhenish massif and the southern Ruhr Basin: New constraints from fission-track analysis, *Int. J. Earth Sci.*, *94*(2), 180–192, doi:10.1007/s00531-005-0467-2.

Ketcham, R. A. (2005), Forward and inverse modeling of low-temperature thermochronometry data, *Rev. Mineral. Geochem.*, *58*(1), 275–314, doi:10.2138/rmg.2005.58.11.

Ketcham, R. A., R. A. Donelick, and W. D. Carlson (1999), Variability of apatite fission-track annealing kinetics: III. Extrapolation to geological time scales, *Am. Mineral.*, *84*, 1235–1255.

Ketcham, R. A., R. A. Donelick, and M. B. Donelick (2000), AFTSolve: A program for multi-kinetic modeling of apatite fission-track data, *Geol. Mater. Res.*, *2*(1), 1–32.

Ketcham, R. A., A. Carter, R. A. Donelick, J. Barbarand, and A. J. Hurford (2007), Improved modeling of fission-track annealing in apatite, *Am. Mineral.*, *92*, 799–810, doi:10.2138/am.2007.2281.

Kley, J., and T. Voigt (2008), Late Cretaceous intraplate thrusting in central Europe: Effect of Africa-Iberia-Europe convergence, not Alpine collision, *Geology*, *36*(11), 839–842, doi:10.1130/G24930A.1.

Kockel, F. (2003), Inversion structures in central Europe—Expressions and reasons, an open discussion, *Neth. J. Geosci.*, *82*(4), 367–382.
Kuyl, O. (1983), The inversion of part of the southern border of the Central Graben in South Limburg during the Late Cretaceous, *Geol. Mijnbouw*, *16*, 401–408.
Littke, R., C. Buker, M. Hertle, H. Karg, V. Stroetmann-Heinen, and O. Oncken (2000), Heat flow evolution, subsidence and erosion in the Rheno-Hercynian orogenic wedge of central Europe, *Geol. Soc. Spec. Publ.*, *179*(1), 231–255, doi:10.1144/GSL.SP.2000.179.01.15.
Luijendijk, E., M. ter Voorde, R. T. van Balen, H. Verweij, and E. Simmelink (2011), Thermal state of the Roer Valley Graben, part of the European Cenozoic Rift System, *Basin Res.*, *23*(1), 65–82, doi:10.1111/j.1365-2117.2010.00466.x.
Meyer, W., and J. Stets (1998), Junge Tektonik im Rheinischen Schiefergebirge und ihre Quantifizierung, *Z. Dtsch. Ges. Geowiss. ZDGG*, *149*(3), 359–379.
Michon, L., R. T. Van Balen, O. Merle, and H. Pagnier (2003), The Cenozoic evolution of the Roer Valley Rift System integrated at a European scale, *Tectonophysics*, *367*(1–2), 101–126, doi:10.1016/S0040-1951(03)00132-X.
Muchez, P. (1995), Geochemical constraints on the origin and migration of palaeofluids at the northern margin of the Variscan foreland, southern Belgium, *Sediment. Geol.*, *96*(3–4), 191–200, doi:10.1016/0037-0738(94)00118-E.
Nelder, J. A., and R. Mead (1965), A simplex method for function minimization, *Comput. J.*, *7*(4), 308–313.
Nielsen, S. B., and D. L. Hansen (2000), Physical explanation of the formation and evolution of inversion zones and marginal troughs, *Geology*, *28*(10), 875–878.
Nielsen, S. B., E. Thomsen, D. L. Hansen, and O. R. Clausen (2005), Plate-wide stress relaxation explains European Palaeocene basin inversions, *Nature*, *435*(7039), 195–198, doi:10.1038/nature03599.
Rohrman, M., P. Andriessen, and P. Van der Beek (1996), The relationship between basin and margin thermal evolution assessed by fission track thermochronology: An application to offshore southern Norway, *Basin Res.*, *8*(1), 45–63.
Sclater, J., and P. Christie (1980), Continental stretching: An explanation of the post-mid-Cretaceous subsidence of the central North Sea Basin, *J. Geophys. Res.*, *85*(B7), 3711–3739.
Senglaub, Y., M. Brix, A. Adriasola, and R. Littke (2005), New information on the thermal history of the southwestern Lower Saxony Basin, northern Germany, based on fission track analysis, *Int. J. Earth Sci.*, *94*(5), 876–896, doi:10.1007/s00531-005-0008-z.
Sissingh, W. (2004), Palaeozoic and Mesozoic igneous activity in the Netherlands: A tectonomagmatic review, *Neth. J. Geosci.*, *83*(2), 113–134.
Steckler, M., and A. Watts (1978), Subsidence of the Atlantic-type continental margin off New York, *Earth Planet. Sci. Lett.*, *41*(1), 1–13, doi:10.1016/0012-821X(78)90036-5.
Teichmuller, M., and R. Teichmuller (1971), Das Revier von Aachen-Erkelenz, b. Inkohlung, *Fortschr. Geol. Rheinl. Westfalen*, *19*, 69–72.
Van Adrichem Boogaert, H. A., and W. F. Kouwe (1997), *Stratigraphic Nomenclature of the Netherlands, Revision and Update by RGD and NOGEPA*, *Meded. Rijks Geol. Dienst*, *50*.
Van Balen, R. T., Y. Y. Podladchikov, and S. A. P. L. Cloetingh (1998), A new multilayered model for intraplate stress-induced differential subsidence of faulted lithosphere, applied to rifted basins, *Tectonics*, *17*(6), 938–954, doi:10.1029/1998TC900003.
Van Balen, R. T., F. van Bergen, C. de Leeuw, H. Pagnier, H. Simmelink, J. D. van Wees, and J. M. Verweij (2000a), Modelling the hydrocarbon generation and migration in the West Netherlands Basin, the Netherlands, *Geol. Mijnbouw*, *79*, 29–44.
Van Balen, R. T., R. F. Houtgast, F. M. Van der Wateren, J. Vandenberghe, and P. W. Bogaart (2000b), Sediment budget and tectonic evolution of the Meuse catchment in the Ardennes and the Roer Valley Rift System, *Global Planet. Change*, *27*(1–4), 113–129, doi:10.1016/S0921-8181(01)00062-5.
Van Balen, R. T., J. M. Verweij, J. Van Wees, H. Simmelink, F. Van Bergen, and H. Pagnier (2001), Deep subsurface temperatures in the Roer Valley Graben and the Peelblock, the Netherlands new results, *Geol. Mijnbouw*, *81*, 19–26.
Van Balen, R. T., R. F. Houtgast, and S. A. P. L. Cloetingh (2005), Neotectonics of the Netherlands: A review, *Quat. Sci. Rev.*, *24*(3–4), 439–454.
Van Bergen, M. J., and W. Sissingh (2007), Magmatism in the Netherlands: Expression of the north-west European rifting history, in *Geology of the Netherlands*, edited by T. E. Wong, D. A. J. Batjes, and J. De Jager, pp. 197–221, R. Neth. Acad. of Arts and Sci., Amsterdam.
Van Dalfsen, W., J. C. Doornenbal, S. Dortland, and J. Gunnink (2006), VELMOD-1 Joint Industry Project, technical report, TNO Built Environ. and Geosci., Utrecht, Netherlands.
Vandenberghe, N., S. Van Simaeys, E. Steurbaut, J. W. M. Jagt, and P. J. Felder (2004), Stratigraphic architecture of the Upper Cretaceous and Cenozoic along the southern border of the North Sea Basin in Belgium, *Neth. J. Geosci.*, *83*(3), 155–171.
Van der Beek, P., X. Robert, J. L. Mugnier, M. Bernet, P. Huyghe, and E. Labrin (2006), Late Miocene–recent exhumation of the central Himalaya and recycling in the foreland basin assessed by apatite fission-track thermochronology of Siwalik sediments, Nepal, *Basin Res.*, *18*(4), 413–434.
Van Wijhe, D. H. (1987), Structural evolution of inverted basins in the Dutch offshore, *Tectonophysics*, *137*(1–4), 171–175.
Vejbæk, O., and C. Andersen (2002), Post mid-Cretaceous inversion tectonics in the Danish Central Graben—Regionally synchronous tectonic events?, *Bull. Geol. Soc. Den.*, *49*, 129–144.
Verbeek, J. W., C. S. de Leeuw, N. Parker, and T. E. Wong (2002), Characterisation and correlation of Tertiary seismostratigraphic units in the Roer Valley Graben, *Neth. J. Geosci.*, *81*(2), 159–166.
Vercoutere, C., and P. Van den Haute (1993), Post-Palaeozoic cooling and uplift of the Brabant Massif as revealed by apatite fission track analysis, *Geol. Mag.*, *130*(5), 639–646.
Vermeesch, P. (2004), How many grains are needed for a provenance study?, *Earth Planet. Sci. Lett.*, *224*(3–4), 441–451, doi:10.1016/j.epsl.2004.05.037.
Wagner, G. A., and G. M. Reimer (1972), Fission track tectonics: The tectonic interpretation of fission track apatite ages, *Earth Planet. Sci. Lett.*, *14*(2), 263–268, doi:10.1016/0012-821X(72)90018-0.
Winstanley, A. M. (1993), A review of the Triassic play in the Roer Valley Graben, SE onshore Netherlands, in *Petroleum Geology Conference Series*, vol. 4, edited by J. R. Parker, pp. 595–607, Geol. Soc., London.
Wong, T. E. (2007), Jurassic, in *Geology of the Netherlands*, edited by T. E. Wong, D. A. J. Batjes, and J. De Jager, pp. 107–125, R. Neth. Acad. of Arts and Sci., Amsterdam.
Xu, C., J. L. Mansy, P. Van den Haute, F. Guillot, Z. Zhou, J. Chen, and J. De Grave (2009), Late- and post-Variscan evolution of the Ardennes in France and Belgium: Constraints from apatite fission-track data, *Geol. Soc. Spec. Publ.*, *324*(1), 167–179, doi:10.1144/SP324.13.
Ziegler, P. A. (1987), Late Cretaceous and Cenozoic intra-plate compressional deformations in the Alpine foreland—A geodynamic model, *Tectonophysics*, *137*(1–4), 389–420, doi:10.1016/0040-1951(87)90330-1.
Ziegler, P. A. (1990), *Geological Atlas of Western and Central Europe*, 2nd ed., Shell Int. Pet. Maatschappij B.V., The Hague, Netherlands.
Ziegler, P. A. (1992a), Geodynamics of rifting and implications for hydrocarbon habitat, *Tectonophysics*, *215*(1–2), 221–253.
Ziegler, P. A. (1992b), North Sea rift system, *Tectonophysics*, *208*(1–3), 55–75.
Ziegler, P. A., S. A. P. L. Cloetingh, and J. D. Van Wees (1995), Dynamics of intra-plate compressional deformation: The Alpine foreland and other examples, *Tectonophysics*, *252*(1–4), 7–22, doi:10.1016/0040-1951(95)00102-6.
Ziegler, P. A., J. D. Van Wees, and S. A. P. L. Cloetingh (1998), Mechanical controls on collision-related compressional intraplate deformation, *Tectonophysics*, *300*(1–4), 103–129, doi:10.1016/S0040-1951(98)00236-4.
Zijerveld, L., R. Stephenson, S. Cloetingh, E. Duin, and M. W. van den Berg (1992), Subsidence analysis and modelling of the Roer Valley Graben (SE Netherlands), *Tectonophysics*, *208*(1–3), 159–171.

P. A. M. Andriessen, E. Luijendijk, M. Ter Voorde, and R. T. Van Balen, Faculty of Earth and Life Sciences, Vrije Universiteit Amsterdam, De Boelelaan 1085, NL-1081HV, Amsterdam, Netherlands. (paul.andriessen@falw.vu.nl; elco.luijendijk@falw.vu.nl; marlies.ter.voorde@falw.vu.nl; ronald.van.balen@falw.vu.nl)